

Streamwise absolute instability of a three-dimensional boundary layer at high Reynolds numbers

By OLEG S. RYZHOV¹ AND EUGENE D. TERENCEV²

¹Department of Mathematical Sciences, Rensselaer Polytechnic Institute, Troy, NY 12180-3590, USA

²Computing Center, Russian Academy of Sciences, 40 Varilov Street, 117333 Moscow, Russian Federation

(Received 8 April 1997 and in revised form 18 May 1998)

The simplest receptivity problem of linear disturbances artificially excited in a three-dimensional boundary layer adjacent to a solid surface is studied in the framework of the generalized triple-deck theory. In order to provide a mathematical model to be compared with experimental data from wind-tunnel tests we consider the base flow over a swept flat plate. Then crossflow in the near-wall region originates owing to an almost constant pressure gradient induced from outside with a displacement body on top. A pulsed or vibrating ribbon installed on the solid surface serves as an external agency provoking initially weak pulsations. A periodic dependence of the ribbon shape on a coordinate normal to the streamwise direction makes the receptivity problem effectively two-dimensional, thereby allowing a rigorous analysis to be carried out without additional assumptions.

The most striking result from the asymptotic theory is the discovery of streamwise absolute instability intrinsic to a three-dimensional boundary layer at high Reynolds numbers. However, due to limitations imposed on the receptivity problem no definite conclusions can be made with regard to possible continued convection of disturbances in the crossflow direction. An investigation of the dispersion-relation roots points to the fact that wave packets of different kinds can be generated by an external source operating in the pulse mode. Rapidly growing wave packets sweep downstream, weaker wave packets move against the oncoming stream. Insofar as the amplitude of all of the modulated signals increases exponentially in time and space, the excitation process gives rise to absolutely unstable disturbances in the streamwise direction. The computation confirms the theoretical prediction about the existence of upstream-advancing wave packets. They can be prevented from being persistently amplified only in a region ahead of the ribbon where nearly critical values of the Reynolds number are attained.

The results achieved are shown to be broadly consistent with wind-tunnel measurements. Hence a conjecture is made that the onset of transition is probably associated, under some environmental conditions, with the mechanism of streamwise absolute instability in the supercritical range of the Reynolds numbers.

1. Introduction

Instability of three-dimensional boundary layers is an area rich in contradictions between theory and experiment. What is more, on occasion experimentalists do

not agree with each other when treating results of wind-tunnel measurements. This situation was building up gradually and acquired an acute form in the last few years. A remarkable property was revealed in the first observations by Gray (1952) in flight tests with a boundary layer on a yawed wing. He found closely spaced stationary streaks in the direction of a local external stream at the upper reaches of the boundary layer. This discovery was at variance with common experience coming from two-dimensional studies, both theoretical and experimental, where the boundary-layer instability manifests itself through self-excited Tollmien–Schlichting (TS) waves. Three years later Gregory, Stuart & Walker (1955) provided an explanation for a stationary mode of crossflow vortices to exist in the context of linear hydrodynamic stability theory. Since that time the dominant role played by crossflow vortex structures was repeatedly reported in independent investigations of the American (Saric & Yeates 1985), British (Poll 1985), Japanese (Kohama 1987), French (Arnal & Juillen 1987) and German (Nitschke-Kowsky & Bippes 1988) groups of scientists who used facilities with various free-stream-turbulence levels as well as different set-ups. The principle feature intrinsic to crossflow instability was seemingly clarified by these findings. It might be worth mentioning that china-clay visualization techniques as well as hot-wire measurements used in experimental studies show only repeatable disturbances. Neither of two methods can detect the presence of travelling waves excited by free-stream turbulence in flight and wind-tunnel tests. Evidently, random disturbances do not appear in visualization footprints, similarly they cancel out when time series are ensemble averaged to improve the signal-to-noise ratio in hot-wire records. This seems to be a possible reason for stationary disturbances being observed predominantly in early investigations.

However, coexisting travelling waves were registered also; according to Poll (1985) and Nitschke-Kowsky & Bippes (1988) they appear almost simultaneously at the same chordwise station as where the crossflow vortices start developing. The subsequent work of Dallman & Bieler (1987) showed that these two instability modes may be of equal significance in the transitional process on a swept wing and the most rapidly amplifying disturbances are even travelling waves rather than stationary vortices. This conclusion from the linear analysis gave rise to a controversy between theory and experiment which, until recently, was regarded to be the main one because stationary streaks in the direction of a local external stream often dominate, as mentioned above, the disturbance field in three-dimensional boundary layers both in flight and wind-tunnel tests. A more detailed comparison of wind-tunnel measurements with theoretical predictions led to a similar contradictory picture. The observed frequencies of the unsteady eigenmodes and the wavelengths of the stationary crossflow modes were in good agreement with the linear stability analysis by Dallman & Bieler (1987). On the other hand, the linear approach largely overestimated the amplitude growth rates of the unsteady eigenmodes coming into play as a primary instability. For this reason Reed & Saric (1989) have not only called into question the very validity of hydrodynamic stability theory as applied to three-dimensional boundary-layer flows but argued that in the general three-dimensional case, as opposed to the two-dimensional one, the theory was apparently not well posed.

Further experimental evidence was necessary to settle the matter. This came from two sources. First, a thorough study of the stationary crossflow vortex modes with artificially controlled disturbances on a swept flat plate surface was undertaken by Kachanov, Tararykin & Fedorov (1990). In principle, this technique can provide extremely conclusive data. Secondly, the amplification of both stationary and unsteady eigenmodes in a similar boundary layer under conditions of natural environmental

disturbances in two wind tunnels with different levels of free-stream turbulence was measured by Bippes, Müller & Wagner (1991). It turned out that the amplification rates of the stationary vortex modes excited in low-turbulence wind tunnels were fairly well predicted on the basis of linear stability analysis for both sets of independent experiments, lending some credence to the validity of this approach. The findings of both groups of experimentalists cleared away grave doubts about hydrodynamic stability theory being ill posed in a finite Reynolds number range even if the velocity field is of the general three-dimensional character. On the other hand, according to Bippes *et al.* (1991) the initial growth of the unsteady modes prior to the beginning of saturation was still essentially overestimated. They emphasized also that the dominant mode could be switched from stationary to travelling when the free-stream turbulence level increased. In a recent work by Deyhle & Bippes (1996) the travelling modes were observed for the first time to be more amplified than the stationary modes as expected from local stability analysis in Dallman & Bieler (1987).

The next step was due to Deyhle, Höhler & Bippes (1993) and Radeztsky *et al.* (1993). The purpose was to obtain additional data on travelling waves developing under natural environmental conditions and crossflow receptivity to micron-sized roughness elements. Deyhle *et al.* (1993) found that the directions of propagation, phase velocities and wavelengths of monochromatic travelling disturbances as predicted by linear stability calculations fitted well with their experimental results. Hydrodynamic stability theory was confirmed to be valid as applied to unsteady modes excited in the three-dimensional boundary layer on a swept wing. As for the group velocities, significant differences appeared in computed and observed directions, ranging up to 30–40°. Then, cleaning the wing surface between test runs changed the spanwise location of stationary vortices that were provoked in the natural transition experiment by tiny roughnesses. Thus, the position from where the crossflow vortices start growing turned out to be extremely sensitive even to minor scratches and other surface imperfections. This effect was thoroughly studied by Radeztsky *et al.* (1993) using micron-sized artificial roughness elements near the attachment line on a swept wing. In point of fact, their contribution to the archival database was designed to provide a deeper insight into receptivity, one of the key missing ingredients in most of the three-dimensional boundary-layer tests discussed above. The receptivity process for stationary crossflow vortices proved to be strongly influenced by surface unevenness from the vicinity of the attachment line. On the other hand, the same micron-sized obstacles had no effect on travelling waves in the streamwise direction. Contrary to Kachanov *et al.* (1990), Bippes *et al.* (1991) and Deyhle *et al.* (1993), in a later paper Radeztsky, Reibert & Saric (1994) claimed that hydrodynamic stability theory failed to correctly yield the growth rates for stationary crossflow modes to the degree that the amplification curves did not even have the correct sign. Recent observations by Deyhle & Bippes (1996) seem to be also at variance with this extreme standpoint. They found the strongest receptivity of the three-dimensional boundary layer to fall within the region of neutral stability for a spacing of roughness elements equivalent to the most unstable stationary vortex wavelength and a certain diameter of disturbing dots. According to Deyhle & Bippes (1996) the most amplified vortices prevailed independent of the stimulated wavenumbers.

In order to most clearly demonstrate the state of the art in the field of three-dimensional boundary-layer transition to turbulence, it is pertinent to present two citations from current reviews written by leading scientists on the basis of numerous experimental results. The statement by Kachanov (1996) summarizing the work of the Novosibirsk team reads: ‘Everything is OK with the linear stability theory as

applied to the swept-wing boundary layer'. At the same time Reed, Saric & Arnal (1996) arrive at exactly the opposite conclusion: 'Linear theory often predicts strong growth (of stationary crossflow waves) where the amplitude is actually decaying'. Due to controversies in experimental findings obtained by different groups of investigators in Germany, Russia and the US the problem of the swept-wing boundary-layer instability appears to be even more intricate than it seemed a few years before. Therefore, it seems likely that some basic concept was missing from the consideration of this problem.

The work on a related problem on the rotating-disk flow led to a similar contradictory picture. We mention here only a few issues relevant to the above discussion and note that from the theoretical point of view the rotating-disk boundary layer is even more attractive because mean flow admits an explicit solution. According to Wilkinson & Malik (1985), the stationary vortex modes originated at discrete sites of minute randomly-distributed dust particles on the disk surface (cf. the aforementioned wind-tunnel tests by Deyhle *et al.* 1993 with the swept-wing flow past the same model cleaned between successive runs). The downstream developing spiral-vortex pattern was the result of interfering zero-frequency disturbances arising from randomly-distributed sources. However, the key observation by Wilkinson & Malik (1985) was on the effect of a single isolated surface imperfection. They recorded the growth of stationary waves which rapidly spread around the disk to eventually fill the entire circumference. The transition Reynolds number based on hot-wire evidence of turbulent breakdown fell in a slightly lower range for the disk with a single three-dimensional roughness element compared to the plain disk with no artificial unevennesses. The sensitivity of the rotating-disk flow to minute surface-roughness elements was further examined by Corke & Knasiak (1996). The periodic roughness in the form of discrete ink dots on the disk surface focused disturbance energy into an initially narrow band of travelling eigenmodes. Their amplitude was observed to be in line with the predictions from linear analysis and approximately 2–3 times larger than the stationary vortex modes following the dots.

Despite an extremely strong response of the rotating-disk boundary layer to surface imperfections, the onset of transition, as found by various experimentalists, takes place consistently at the critical Reynolds number of about 513 showing a small scatter of less than 3% around an average value. What is more, the critical Reynolds number is the same with and without artificial excitation of the base flow. This property led Lingwood (1995) to advance a conceptually new idea that could reconcile the contradictions inherent in both theoretical and experimental studies of the three-dimensional boundary-layer instabilities. The lack of sensitivity to the form of the disturbance environment was conjectured in her analysis to be indicative of an absolutely unstable velocity field. Worthy of mention is also an earlier survey by Huerre & Monkewitz (1990) where they exposed strong evidence signalling the likelihood that absolute and global instabilities do arise in shear flows of various kinds. Sources of different physical nature can trigger absolutely unstable disturbances to grow following different scenarios but terminate in the same transition-to-turbulence state, which is governed by nonlinear effects coming into play at the same critical Reynolds number. In order to substantiate the concept of absolute instability, as applied to the rotating-disk flow, Lingwood (1995) used a criterion from the work of Briggs (1964) and Bers (1975) on plasma physics. Absolute instability was identified by evaluating singularities in the complex wavenumber plane of the dispersion relation, which are known as pinch-points. The crucial role in their formation turned out to belong to two branches of the dispersion-relation roots. One of the branches

comprises the non-zero-frequency crossflow modes whereas the other branch relates to the spatially damped modes briefly mentioned by Mack (1985) and Balakumar & Malik (1990). The radial component of the group-velocity vector becomes identically zero at the pinch-point. In a subsequent study by Lingwood (1996), the radial propagation of the trailing edge of the wave packet impulsively excited by a point source was directly observed to tend to zero as it approached a position fixed by the critical Reynolds number.

As is evident from what has been said above the problem of the paths to transition in a three-dimensional boundary layer has to be put on a firm footing of a rational mathematical analysis embracing the entire disturbance pattern. The linear stability theory appears to offer a reliable basis, because all the data available testify that the frequencies and wavenumbers of both stationary and unsteady eigenmodes belong to the TS wave range. The amplitude growth rates cannot be properly estimated using either temporal or spatial conventional approaches if the boundary layer is absolutely unstable. Thus, the feasibility upstream of propagating wave packets is to be anticipated when we set about solving the linear problem. The concept of an interactive boundary layer, where the pressure variations and the instantaneous displacement thickness are evaluated simultaneously, seems to be best suited for our purposes. Asymptotic simplifications arising within the framework of the triple-deck scheme were discussed by Manuilovich (1983), Stewart & Smith (1987) and Ryzhov & Terent'ev (1991). The classical version of the triple deck turned out to possess an inherent flaw in the form of a strong singularity making the Cauchy problem ill posed in the linear approximation. To remove the singularity, Ryzhov & Terent'ev (1996, 1997) generalized the triple-deck theory by accounting for the normal pressure gradient supported by centrifugal forces due to the streamsurface warping in the crossflow direction. A new version of the asymptotic model involves the Reynolds-number dependence in an explicit manner.

In the work set forth below receptivity is regarded to be the key issue in resolving the aforementioned contradictions intrinsic to the study of the three-dimensional boundary layer on a swept wing. To this end, the extended triple-deck theory developed by Ryzhov & Terent'ev (1996, 1997) is employed to pose the problem of disturbances excited by a vibrating ribbon on an otherwise flat plate. The simple geometry of a solid body in the asymptotic model is chosen to conform to a special experimental technique which has been invented to discriminate between Görtler vortices evolving on a concave surface and crossflow vortices peculiar to any swept-wing flow (Saric & Yeates 1985; Kachanov *et al.* 1990). Insofar as the surface curvature becomes identically zero in the case of a flat plate, generation of the Görtler vortices is completely suppressed. A periodic dependence of the ribbon shape on the spanwise coordinate makes the receptivity problem effectively two-dimensional, thereby allowing a rigorous analysis to be carried out along the lines described in Ryzhov & Terent'ev (1984, 1986), without additional assumptions. In particular, we do not resort to the Briggs–Bers criterion for determining pinch-points. Instead, computed directions of the group velocity are at the bottom of our analysis pointing to the existence, within certain limits, of wave packets endowed with disparate properties. The rapidly growing wave packets sweep downstream of a disturbing source, the weaker wave packets propagate upstream. However, the amplitude of the latter, highly modulated, signals also increases exponentially in time and space. As a consequence, the excitation process gives rise to absolutely unstable disturbances in the streamwise direction, ahead of the vibrating ribbon. On the other hand, due to constraints imposed on the receptivity problem no definite conclusions can be drawn with regard to possible

continued convection of disturbances in the crossflow direction. The problem of a point source should be addressed to bring to light the absolute instability in the strict sense, i.e. simultaneously developing both in the streamwise and crossflow directions (Huerre & Monkewitz 1990). The latter problem is attacked by Lingwood (1997) and Taylor & Peake (1998) in recent studies that appeared when the present paper was in the process of being reviewed. According to Lingwood (1997), disturbances from the point source are absolutely unstable in the chordwise direction on the wing surface but free to drift in the spanwise direction. This distinctive feature of exponentially amplifying waves is referred to by Lingwood (1997) as 'chordwise absolute instability' pointing to the essence of the matter. The term 'streamwise absolute instability' is used here in an analogous way. Taylor & Peake (1998) demonstrate further that there exists a range of directions where the group-velocity vector can be resolved into components endowed with similar properties. In projection on a direction falling within this range the group velocity has a component vanishing to zero while the other component remains finite. In particular, in order to fix the direction of maximum growth close to the leading edge of a wing, they resolve the velocity profiles away from the streamwise/crossflow direction towards the chordwise/spanwise direction.

The mechanism under discussion is peculiar to the three-dimensional boundary layer where the direction of the wall shear differs from the direction of a streamline in the local outer stream. In the two-dimensional boundary layer both directions coincide to suppress the upstream motion of wave packets. The amplification of the upstream advancing disturbance must eventually make the linear approximation break down as time passes after launching the disturbing ribbon. Thus, the linear theory proves to be appropriate for predicting streamwise absolute instability of a three-dimensional boundary layer with crossflow but incapable of determining its final state in the vicinity of a vibrator operating in the supercritical Reynolds-number range.

Our concern is mainly with the aforementioned basic mechanism controlling the upstream propagation of disturbances. We start in §2 with posing the receptivity problem on a vibrating ribbon impulsively put into operation at some initial moment. Taking account of centrifugal forces in the interaction law allows us to damp an excessively high growth of eigenmodes with large spanwise wavenumbers. The receptivity problem simplifies in a linear approximation considered in §3 on the assumption that the vibrating ribbon amplitude is small enough. Then the Laplace–Fourier transform in time and streamwise coordinate provides a solution to the linear problem in an explicit form. With real values of both wavenumbers, all the singularities in final expressions for desired functions are reduced to a countable set of poles in the complex frequency plane which derive from the dispersion-relation roots. An analysis of the dispersion curves in the whole plane presented in §4 is the cornerstone of the work. It shows that the first dispersion curve associated with unstable oscillations splits into two separate branches. In turn, each of the branches consists of two lobes merging together. The lower and upper lobes which pass close to the imaginary axis are inherent only in the three-dimensional boundary layers with crossflow and cease to exist when the velocity field becomes two-dimensional. These lobes may be treated as counterparts of spatially damped modes from Mack (1985), Balakumar & Malik (1990) and Lingwood (1995) but in the complex frequency plane they represent exponentially enhancing disturbances. There is a range of the crossflow wavenumbers where the lower lobe has a fairly strong peak in the real part of complex frequencies. Since the value of the group velocity at the location of this peak is negative, it sets up a wave packet advancing upstream of the vibrating ribbon. Time-dependent fields of

the self-induced pressure are discussed in §5. We start with periodic oscillations in the vicinity of the ribbon. For the sake of simplicity, highly modulated signals are considered on the assumption that the time is large enough. Downstream sweeping, rapidly amplifying wave packets provoke convective instability and conventional routes to transition. Computed results illustrate also the disturbance patterns that evolve ahead of the vibrating ribbon depending on the value of the crossflow wavenumber. Despite their lower amplitudes, the upstream advancing wave packets are shown to be dangerous disturbances since they give rise to streamwise absolute instability and may be of importance for the transition process. Concluding remarks in §6 are of two kinds: they demonstrate a broad consistency of the conclusions from the asymptotic analysis developed and indicate limitations on streamwise absolute instability being a dominant mechanism in the path to transition under various environmental circumstances.

2. Receptivity problem

The base motion to be considered below is a general steady three-dimensional boundary layer with the Mach number $M_\infty < 1$ at the outer edge. The triple deck is chosen to describe lower-branch instabilities in the form of self-excited TS waves and crossflow vortex modes which can be coupled together. As usual for this asymptotic approach, we introduce a small parameter $\varepsilon = R^{-1/8}$, where the local Reynolds number $R \gg 1$ is based on a reference length L^* associated with a particular position (x_0^*, z_0^*) on a swept flat plate, the free-stream velocity U_∞^* , density ρ_∞^* and viscosity μ_∞^* just outside the boundary layer. Cartesian coordinates (x', y', z') are non-dimensionalized with L^* ; according to a definition most commonly in use, the x' -axis is aligned with the direction of the local external stream, y' stands for the normal-to-wall distance and z' indicates the local crossflow direction (Reed & Saric 1989; Reed *et al.* 1996). The corresponding non-dimensional velocities (u', v', w') are based on U_∞^* . Their profiles $U_{x0}(y_2)$, 0 , $U_{z0}(y_2)$, depending on a scaled distance $y' = \varepsilon^4 y_2$ within the undisturbed boundary layer, are evaluated on the assumption that adiabatic conditions hold at the thermally insulated solid surface. In the frame of reference adopted, the crossflow $U_{z0} \rightarrow 0$ as $y_2 \rightarrow \infty$; however both normalized wall shear stresses

$$\tau_x \tau_w = C^{1/2} \frac{T_w^*}{T_\infty^*} \frac{dU_{x0}(0)}{dy_2}, \quad \tau_z \tau_w = C^{1/2} \frac{T_w^*}{T_\infty^*} \frac{dU_{z0}(0)}{dy_2} \quad (2.1a,b)$$

are non-zero. The frictional intensity

$$\tau_w = C^{1/2} \frac{T_w^*}{T_\infty^*} \left[\left(\frac{dU_{x0}(0)}{dy_2} \right)^2 + \left(\frac{dU_{z0}(0)}{dy_2} \right)^2 \right]^{1/2} \quad (2.2)$$

entering (2.1a, b) varies linearly with the ratio T_w^*/T_∞^* of the wall temperature T_w^* to the temperature T_∞^* in the local external stream provided that advantage is taken of the Chapman viscosity law with a constant denoted by C .

The present problem setting starts with the conventional triple-deck scales for the near-wall viscous sublayer. With the time t' non-dimensionalized with respect to L^*/U_∞^* , we introduce the following independent variables:

$$t' = \varepsilon^2 \tau_w^{-3/2} C^{1/4} (T_w^*/T_\infty^*) t, \quad (2.3a)$$

$$(x' - x'_0, z' - z'_0) = \varepsilon^3 \tau_w^{-5/4} C^{3/8} (T_w^*/T_\infty^*)^{3/2} (x, z), \quad (2.3b)$$

$$y' = \varepsilon^5 \tau_w^{-3/4} C^{5/8} (T_w^*/T_\infty^*)^{3/2} y, \quad (2.3c)$$

where $x'_0 = x_0^*/L^*$, $z'_0 = z_0^*/L^*$ and τ_w comes from (2.2). The free-stream values ρ_∞^* and $\rho_\infty^* U_\infty^{*2}$ are used to obtain the non-dimensional density ρ' and excess pressure p' . Then, the scaled and normalized desired functions are defined by

$$(u', w') = \varepsilon \tau_w^{1/4} C^{1/8} (T_w^*/T_\infty^*)^{1/2} (\tilde{u}, \tilde{w}), \quad (2.4a)$$

$$v' = \varepsilon^3 \tau_w^{3/4} C^{3/8} (T_w^*/T_\infty^*)^{1/2} \tilde{v}, \quad (2.4b)$$

$$p' = \varepsilon^2 \tau_w^{1/2} C^{1/4} \tilde{p}, \quad (2.4c)$$

whereas the density $\rho' = (T_w^*/T_\infty^*)^{-1}$ is held constant (see for example Stewartson 1969; Messiter 1970; Smith, Sykes & Brighton 1977; Stewart & Smith 1987). On the other hand, in most of the boundary layer the density profile $R_0(y_2)$ varies with the normal-to-wall distance y_2 , an obvious constraint for the thermally insulated surface being $dR_0(0)/dy_2 = 0$. On substitution of (2.3a–c) and (2.4a–c) into the initial Navier–Stokes equations we are left with a simpler system of the Prandtl equations

$$\frac{\partial \tilde{u}}{\partial x} + \frac{\partial \tilde{v}}{\partial y} + \frac{\partial \tilde{w}}{\partial z} = 0, \quad (2.5a)$$

$$\frac{\partial \tilde{u}}{\partial t} + \tilde{u} \frac{\partial \tilde{u}}{\partial x} + \tilde{v} \frac{\partial \tilde{u}}{\partial y} + \tilde{w} \frac{\partial \tilde{u}}{\partial z} = -\frac{\partial \tilde{p}}{\partial x} + \frac{\partial^2 \tilde{u}}{\partial y^2}, \quad (2.5b)$$

$$\frac{\partial \tilde{w}}{\partial t} + \tilde{u} \frac{\partial \tilde{w}}{\partial x} + \tilde{v} \frac{\partial \tilde{w}}{\partial y} + \tilde{w} \frac{\partial \tilde{w}}{\partial z} = -\frac{\partial \tilde{p}}{\partial z} + \frac{\partial \tilde{w}}{\partial y^2}, \quad (2.5c)$$

for an incompressible boundary layer where both spatial derivatives $\partial \tilde{p}/\partial x$ and $\partial \tilde{p}/\partial z$ of the self-induced pressure are to be determined simultaneously with the velocity field.

In keeping with the traditional version of the triple deck we have $\partial \tilde{p}/\partial y = 0$. However, there is a distinction between an extended triple-deck approach and the conventional theory which derives from the interaction law relating the excess pressure \tilde{p} to the instantaneous displacement thickness $-\tilde{A}$. In the context of the generalized triple-deck theory the interaction law reads (Ryzhov & Terent'ev 1996, 1997)

$$\tilde{p} = -\frac{1}{2\pi} \int_{-\infty}^{\infty} d\xi \int_{-\infty}^{\infty} \frac{\partial^2 \tilde{A}(t, \xi, \zeta)/\partial \xi^2}{[(1 - M_\infty^2)(x - \xi)^2 + (z - \zeta)^2]^{1/2}} d\zeta - \varepsilon_2 D_{(zz)} \frac{\partial^2 \tilde{A}}{\partial z^2}, \quad (2.6a)$$

$$\varepsilon_2 = \varepsilon \tau_w^{5/4} C^{-3/8} (T_w^*/T_\infty^*)^{-3/2}. \quad (2.6b)$$

Thus, along with the leading, $O(1)$, integral term on the right-hand side (2.6a) includes also the main second-order term proportional to the small parameter ε . The latter term comes from a contribution to the normal pressure gradient from centrifugal forces due to the streamsurface curvature $\partial^2 \tilde{A}/\partial z^2$ in the spanwise direction. A coefficient

$$D_{(zz)} = \int_{-\infty}^{\infty} R_0(y_2) U_{z0}^2(y_2) dy_2 \quad (2.7)$$

can be identified with the spanwise momentum thickness of a three-dimensional boundary layer; it becomes zero in the absence of crossflow U_{z0} . Without the second-order term incorporated into the interaction law (2.6a, b), (2.7), the amplitude growth rate of crossflow eigenmodes proves to increase without bound in the limit as values of both wavenumbers in the (x, z) -plane tend to infinity along certain curves. Because

of this the Cauchy problem is ill posed for the linearized Prandtl equations (Ryzhov & Terent'ev 1991). Accounting for the second-order term in (2.6a) allows us to damp out the aforementioned unrealistic amplification of self-excited disturbances with a consequence that the Cauchy problem becomes regular in a linear approximation. In the framework of the generalized approach under discussion the triple-deck scheme as a whole is preserved intact and simplifies in limiting cases (Ryzhov & Terent'ev 1996, 1997). In particular, at the upper reaches of the near-wall viscous sublayer we have

$$\tilde{u} - \tau_x y \rightarrow \tau_x \tilde{A}, \quad \tilde{w} - \tau_z y \rightarrow \tau_z \tilde{A} \quad \text{as } y \rightarrow \infty \quad (2.8a,b)$$

with the displacement thickness $-\tilde{A}$ arising from viscous-inviscid interaction.

Let us consider a simple receptivity problem where disturbances are supposed to be induced by a vibrating ribbon brought into operation in a pulse mode. The problem seems to be best suited to elucidating the strong response of the three-dimensional boundary layer to an excitation often in use by experimentalists to control the input conditions. They consider incorporating the receptivity into stability analysis as the major issue for future work (Deyhle & Bippes 1996; Reed *et al.* 1996). The formulation with a vibrating ribbon allows us to trace the growth of wave packets generated when triggering an external source and the evolution of time-periodic oscillations continuously fed by the subsequent monochromatic motion of the same source. The periodic oscillations occupy the space between the ribbon and wave packets and can extend in both directions, downstream as well as upstream. Note that impulsively excited wave packets have the spectrum of frequencies, which necessarily contains the most amplified linear mode, whereas in general the harmonic excitation is not chosen to be the most amplified. For this reason, the wave packets may be envisioned as disturbances vigorously building up in time and space.

In the analysis below we concentrate on wave systems emitted during the initial pulse motion of the ribbon. To attain this goal, the ribbon is specified by

$$y = y_w = \begin{cases} \delta \sin(\omega_0 t) f(x) \cos(m_0 z), & t \geq 0 \\ 0, & t < 0 \end{cases} \quad (2.9)$$

with a function $f(x)$ being effectively non-zero only within a finite interval; f will be defined more precisely below. The harmonic dependence of y_w on z adopted serves to simulate experimental set-ups exploiting artificial perturbations in wind-tunnel tests (Saric & Yeates 1985; Kachanov 1996; Deyhle & Bippes 1996). By no means does the mathematical model at hand embrace the free-stream excitation of an in-flight boundary layer which is a more complicated process. A value of the wavenumber m_0 directly relates to the crossflow spacing of artificial devices provoking alternating peaks and drops of the ribbon shape in the same direction. The disturbing agency amplitude is fixed by δ ; in the linear approximation to be developed in the following analysis we assume $\delta \ll 1$.

The boundary conditions at the moving surface are

$$\tilde{u} = \tilde{w} = 0, \quad \tilde{v} = \frac{\partial y_w}{\partial t} \quad \text{at } y = y_w \quad (2.10a,b)$$

where y_w is given in (2.9). In the receptivity problem posed, it is natural to choose initial data in the form

$$\tilde{u} = \tilde{w} = 0 \quad \text{at } t = 0 \quad (2.11)$$

in order to observe the birth and development of various types of disturbances intro-

duced in the three-dimensional boundary layer by the switching on and subsequent monochromatic motion of a narrow ribbon stretching in the crossflow direction.

It is pertinent to emphasize a distinction between the receptivity problem under consideration and that analysed by Lingwood (1995) in connection with the rotating-disk flow. The ribbon in (2.9) extends in the crossflow direction, therefore the group-velocity vector is parallel to the direction of the local outer stream. This formulation may be considered as characteristic of the swept-wing boundary layer. On the other hand, the initial perturbation in Lingwood (1995) is provided by an impulsive circumferential forcing in the form of the Dirac delta function. Evidently, the forcing is aligned with the direction of the oncoming mainflow in a frame of reference rotating with a disk and the group velocity of an excited wave packet is in the radial direction of crossflow. The trailing edge of the wave packet stops moving outwards at a position where the group velocity becomes zero. The rotating-disk boundary-layer breaks down owing to the absolute instability developing in the crossflow direction. On the other hand, the receptivity problem in (2.9), (2.10a, b) is designed to demonstrate the wave patterns evolving due to distinctive instabilities in the streamwise motion of the swept-wing boundary layer. Thus, the receptivity problem posed is indicative only of the streamwise absolute instability. In order to reveal the absolute instability in the strict sense, i.e. in the streamwise and crossflow directions simultaneously, it is necessary to attack the problem of launching a disturbing source where the harmonic dependence of y_w on z is replaced by a function being non-zero within a finite interval $-z_0 < z < z_0$. In this latter case disturbances are free to convect in the crossflow direction making the large-time three-dimensional impulse response quite dissimilar to the effectively two-dimensional impulse response which takes place with the excitation given in (2.9), (2.10a, b).

3. Linear approximation

The boundary-value problem at hand is essentially nonlinear, therefore it allows us in principle to study wave motion of finite amplitude. However, usually the boundary-layer receptivity means a linear process which is brought about by a weak external source with $\delta \rightarrow 0$. Setting

$$(\tilde{u} - \tau_x y, \tilde{v}, \tilde{w} - \tau_z y, \tilde{p}, \tilde{A}) = \delta(\tau_x u, v, \tau_z w, p, A) \quad (3.1)$$

let us simplify the Prandtl equations (2.5a–c) as well as the boundary conditions (2.8a, b), (2.9), (2.10a, b) and initial data (2.11). According to Ryzhov & Terent'ev (1996, 1997) the resulting linear problem is well posed.

We begin with the no-slip conditions (2.10a, b). With allowance made for (2.9) and (3.1) they reduce to

$$(u, v, w) = [-\sin(\omega_0 t), \omega_0 \cos(\omega_0 t), -\sin(\omega_0 t)] f(x) \operatorname{Re}(e^{im_0 z}) \quad \text{at } y = 0, \quad t \geq 0. \quad (3.2)$$

In line with (3.2) a solution is sought in the form

$$(u, v, w, p, A) = \operatorname{Re} [(u_c, v_c, w_c, p_c, A_c) e^{im_0 z}]. \quad (3.3)$$

Here the desired complex functions u_c, v_c, w_c, p_c, A_c are transformed into the Laplace integral in t and the Fourier integral in x by means of

$$\begin{aligned} & [\bar{u}_c(\omega, k, y), \bar{v}_c(\omega, k, y), \bar{w}_c(\omega, k, y), \bar{p}_c(\omega, k), \bar{A}_c(\omega, k)] \\ &= \int_{-\infty}^{\infty} dx \int_0^{\infty} e^{-(\omega t + ikx)} [u_c(t, x, y), v_c(t, x, y), w_c(t, x, y), p_c(t, x), A_c(t, x)] dt. \end{aligned} \quad (3.4)$$

Substitution of (3.3) and (3.4) into the system of linearized Prandtl equations results in a set of homogeneous ordinary differential equations

$$\frac{d\bar{v}_c}{dy} = -i(k\tau_x\bar{u}_c + m_0\tau_z\bar{w}_c), \quad (3.5a)$$

$$\frac{d^2\bar{u}_c}{dy^2} = [\omega + i(k\tau_x + m_0\tau_z)y]\bar{u}_c + \bar{v}_c + \frac{ik}{\tau_x}\bar{p}_c, \quad (3.5b)$$

$$\frac{d^2\bar{w}_c}{dy^2} = [\omega + i(k\tau_x + m_0\tau_z)y]\bar{w}_c + \bar{v}_c + \frac{im_0}{\tau_z}\bar{p}_c, \quad (3.5c)$$

for the function-images \bar{u}_c , \bar{v}_c , \bar{w}_c , \bar{p}_c , \bar{A}_c insofar as the initial data (2.11) for \bar{u}_c and \bar{w}_c are zero. The limiting conditions (2.8a, b) at infinity lead to

$$\bar{u}_c \rightarrow \bar{A}_c, \quad \bar{w}_c \rightarrow \bar{A}_c \quad \text{as } y \rightarrow \infty. \quad (3.6a,b)$$

A simple relation

$$\bar{p}_c = \frac{k^2\bar{A}_c}{[(1 - M_\infty^2)k^2 + m_0^2]^{1/2}} + \varepsilon_2 m_0^2 D_{(zz)}\bar{A}_c \quad (3.7)$$

between \bar{p}_c entering (3.5b, c) and \bar{A}_c from the right-hand sides of (3.6a, b) comes from the interaction law (2.6a, b) with $D_{(zz)}$ given in (2.7). The no-slip conditions (3.2) become

$$(\bar{u}_c, \bar{v}_c, \bar{w}_c) = (-1, \omega, -1) \frac{\omega_0}{\omega^2 + \omega_0^2} \bar{f}(k) \quad \text{at } y = 0, \quad (3.8)$$

where $\bar{f}(k)$ is a Fourier transform of the vibrator shape $f(x)$.

Let us define a reduced wavenumber $K = k\tau_x + m_0\tau_z$ and introduce a new desired function $F = k\tau_x\bar{u}_c + m_0\tau_z\bar{w}_c$. It satisfies an equation

$$\frac{d^2F}{dy^2} - (\omega + iKy)F = K\bar{v}_c + i(k^2 + m_0^2)\bar{p}_c \quad (3.9)$$

following from (3.5b, c). Being coupled together, (3.5a) and (3.9) constitute a complete set of equations for the two functions F and \bar{v}_c . Upon differentiating (3.9) and eliminating $d\bar{v}_c/dy$ between the resulting expression and (3.5a) we obtain

$$\frac{d^3F}{dy^3} - (\omega + iKy)\frac{dF}{dy} = 0. \quad (3.10)$$

Precisely the same equation controls the propagation of TS waves in a Blasius boundary layer with parameters independent of the spanwise coordinate z . This property is the essence of a transformation by Squire (1933) which remains valid asymptotically, as $\varepsilon \rightarrow 0$, even if a steady three-dimensional motion of a compressible fluid involves crossflow in the local spanwise direction. The limiting condition

$$F \rightarrow K\bar{A}_c \quad \text{as } y \rightarrow \infty \quad (3.11)$$

is a linear combination of (3.6a) and (3.6b). Two constraints to be imposed on F at the moving solid surface are derivable from (3.8) and (3.9); they can be written down as

$$F = -K \frac{\omega_0}{\omega^2 + \omega_0^2} \bar{f}, \quad \frac{d^2F}{dy^2} = i(k^2 + m_0^2)\bar{p}_c \quad \text{at } y = 0. \quad (3.12a,b)$$

The standard technique (see for example Ryzhov & Terent'ev 1984, 1986) which depends upon introducing a new independent variable

$$Y = \Omega + i^{1/3}K^{1/3}y, \quad \Omega = i^{-2/3}\omega K^{-2/3} \quad (3.13a,b)$$

serves to solve the boundary-value problem given in (3.10), (3.11) and (3.12a, b). It should be mentioned that a cut along the positive imaginary semi-axis is drawn in the complex K -plane which separates a single-valued branch of the function $K^{1/3}$ by means of $-3\pi/2 < \arg(K) < \pi/2$ with a consequence that $-\pi/3 \leq \arg(Y) \leq \pi/3$ as $y \rightarrow \infty$. After some algebra we arrive at an expression

$$F = -\frac{\omega_0}{\omega^2 + \omega_0^2} \bar{f}(k) \times \left\{ K + \frac{i^{1/3}(k^2 + m_0^2)}{K^{2/3}I(\Omega)} \frac{k^2[(1 - M_\infty^2)k^2 + m_0^2]^{-1/2} + \varepsilon_2 m_0^2 D_{(zz)}}{\Phi(\Omega) - Q(k, m_0; M_\infty, \varepsilon_2 D_{(zz)}; \tau_x, \tau_z)} \int_\Omega \text{Ai}(Y) dY \right\}, \quad (3.14)$$

where $\text{Ai}(Y)$ designates the Airy function, $\Phi(\Omega)$ and $I(\Omega)$ are defined through its first derivative and improper integral by

$$\Phi(\Omega) = \frac{d \text{Ai}(\Omega)}{dY} [I(\Omega)]^{-1}, \quad I(\Omega) = \int_\Omega^\infty \text{Ai}(Y) dY, \quad (3.15a,b)$$

the quantity $Q(k, m_0; M_\infty, \varepsilon_2 D_{(zz)}; \tau_x, \tau_z)$ stands for

$$Q(k, m_0; M_\infty, \varepsilon_2 D_{(zz)}; \tau_x, \tau_z) = i^{1/3}(k^2 + m_0^2)K^{-5/3} \times \{k^2[(1 - M_\infty^2)k^2 + m_0^2]^{-1/2} + \varepsilon_2 m_0^2 D_{(zz)}\} \quad (3.16)$$

and the square root of $(1 - M_\infty^2)k^2 + m_0^2$ is meant to be positive for all real values of k and m_0 . The corresponding expression

$$\bar{p}_c = -\frac{\omega_0}{\omega^2 + \omega_0^2} \bar{f}(k) \frac{\Phi(\Omega) \{k^2[(1 - M_\infty^2)k^2 + m_0^2]^{-1/2} + \varepsilon_2 m_0^2 D_{(zz)}\}}{\Phi(\Omega) - Q(k, m_0; M_\infty, \varepsilon_2 D_{(zz)}; \tau_x, \tau_z)} \quad (3.17)$$

for the Laplace–Fourier transform of pressure variations arises upon substitution of (3.11) into (3.7) with F expressed by means of (3.14). The normal-to-wall velocity component \bar{v}_c stems from (3.5a) cast in the form $d\bar{v}_c/dy = -iF$. Thus, F may be regarded as an asymptotic representation, as $R \rightarrow \infty$, of the normal Orr–Sommerfeld mode.

However, in order to evaluate the other two velocity components in a plane parallel to the wall we need an auxiliary function $G = -\tau_x \tau_z (\bar{u}_c - \bar{w}_c)$ determined by the inhomogeneous Airy equation

$$\frac{d^2 G}{dY^2} - YG = \frac{i^{1/3}(k\tau_z - m_0\tau_x)\bar{p}_c}{K^{2/3}}$$

subject to homogeneous boundary conditions

$$G = 0 \text{ at } Y = \Omega \text{ and } G \rightarrow 0 \text{ as } Y \rightarrow \infty,$$

which are obtainable from (3.6a, b) and (3.8), respectively. A solution

$$G = \frac{i^{1/3}\pi(k\tau_z - m_0\tau_x)\bar{p}_c}{K^{2/3}} \frac{\text{Ai}(\Omega)\text{Gi}(Y) - \text{Gi}(\Omega)\text{Ai}(Y)}{\text{Ai}(\Omega)} \quad (3.18)$$

to the boundary-value problem posed involves a new function $\text{Gi}(Y)$ from the Handbook by Abramowitz & Stegun (1964). It satisfies the inhomogeneous Airy equation with a constant $-1/\pi$ on the right-hand side and the initial conditions

$\text{Gi}(0) = 3^{-1/2}\text{Ai}(0)$, $d\text{Gi}(0)/dy = -3^{-1/2}d\text{Ai}(0)/dY$. Since, in view of (3.13a), $-\pi/3 \leq \arg(Y) \leq \pi/3$ as $Y \rightarrow \infty$ the asymptotic decay of $\text{Gi}(Y)$ obeys an algebraic law $\text{Gi}(Y) \sim \pi^{-1}Y^{-1} + \dots$ rather than being exponential. Hence we deduce

$$G \rightarrow -\frac{i^{1/3}(k\tau_z - m_0\tau_x)\bar{p}_c}{K^{2/3}} \left(\frac{1}{Y} + \frac{2}{Y^4} + \dots \right) \quad \text{as } Y \rightarrow \infty$$

keeping one more term in the asymptotic expansion for $\text{Gi}(Y)$. With G specified through (3.18), the Laplace–Fourier transforms of horizontal velocity components become

$$\bar{u}_c = \frac{F + m_0G/\tau_x}{K}, \quad \bar{w}_c = \frac{F - kG/\tau_z}{K}. \quad (3.19a,b)$$

Thus, G may be treated as a Squire mode. It is known (see for example Benney & Gustavsson 1981; Criminale & Drazin 1990) that the resonance interaction of the normal Orr–Sommerfeld modes with the Squire mode can occur at the early transient stage and give rise to an enormous increase in the disturbance energy before its eventual exponential damping comes in the subcritical range of parameters involved. The period of algebraic growth presumably plays an important part in provoking laminar–turbulent transition; however this issue will not be pursued in the present study. Therefore, in what follows we confine ourselves to the analysis and calculation of the pressure variations using an explicit expression

$$p_c = \frac{\omega_0 i}{4\pi^2} \int_{-\infty}^{\infty} dk e^{ikx} \bar{f}(k) \{k^2[(1 - M_\infty^2)k^2 + m_0^2]^{-1/2} + \varepsilon_2 m_0^2 D_{(zz)}\} \\ \times \int_{\ell - i\infty}^{\ell + i\infty} d\omega e^{\omega t} \Phi(\Omega)(\omega^2 + \omega_0^2)^{-1} [\Phi(\Omega) - Q(k, m_0; M_\infty, \varepsilon_2 D_{(zz)}; \tau_x, \tau_z)]^{-1} \quad (3.20)$$

for the inverse Laplace–Fourier transform. For a definition of ℓ in the limits of the second improper integral on the right-hand side of (3.20) see, for example, Korn & Korn (1961). Taking advantage of the fact that with real k all the singularities in the complex ω -plane are reduced to a countable set of poles, it seems advisable to expand the inverse Laplace transform into series in residues of the integrand at these points. We emphasize that the complex k -plane is far more intricate and contains branch-point singularities in addition to a countable set of poles. As usual, branch points entail the existence of a continuous spectrum of eigen-values coming from their respective brunch-cuts.

4. Dispersion-relation roots

Thus, all the zeros of the denominator in an expression for the integrand are to be traced first of all in the complex ω -plane with k running through an infinite interval $-\infty < k < \infty$. Two fixed zeros

$$\omega^{(\pm)} = \pm i\omega_0 \quad (4.1)$$

are obvious. The other zeros are determined by a dispersion relation

$$\Phi(\Omega) = Q(k, m_0; M_\infty, \varepsilon_2 D_{(zz)}; \tau_x, \tau_z). \quad (4.2)$$

Here $\Phi(\Omega)$, as defined in (3.15a, b), is a standard function inherent in the triple-deck approach to hydrodynamic stability theory (see for example Ryzhov & Terent'ev 1986, 1991, 1997). The dependence of Q on k and five parameters $m_0; M_\infty, \varepsilon_2 D_{(zz)}; \tau_x, \tau_z$ comes from (3.16). We put $M_\infty = 0.2$ to deal with the typical low-Mach-number regime of a compressible fluid and choose $\omega_0 = 3, \tau_x = 2\sqrt{2}/3, \tau_z = 1/3$

as characteristic values for a general three-dimensional boundary layer. The product $\varepsilon_2 D_{(zz)}$ is assumed to take a value $\varepsilon_2 D_{(zz)} = 0.01$. The crossflow wavenumber m_0 is allowed to vary within an interval $0 \leq m_0 \leq 9$. With the parameter range specified in this way, we cover all the essential properties of the streamwise TS modes coupled with crossflow modes. It is just this coupling which gives rise to a specific eigenmode responsible for streamwise absolute instability. However, one needs to bear in mind that the occurrence of critical layers is fully ignored within the framework of the triple-deck scheme under consideration. No indication for the critical layers to be necessarily introduced into the disturbance pattern comes from the analysis of the self-induced pressure as defined in (3.17) and (3.20) because $\partial \tilde{p} / \partial y = 0$ in equations governing the fluid motion. On the other hand, the Laplace–Fourier transforms of the horizontal velocities \bar{u}_c and \bar{w}_c given by (3.19*a, b*) where F and G are to be evaluated through (3.14) and (3.18), respectively, point to a singularity arising in the limit, as $K \rightarrow 0$. This singularity causes a critical layer to be formed in the proximity of the wall. Critical layers of the other kind appear also at a finite distance from the wall as a consequence of the fact that the velocity profile $kU_{x0}(y_2) + m_0 U_{z0}(y_2)$ in the direction of the normal mode propagation can vanish at some point $y_2 = y_{2c}$ inside the main deck if $k < 0$. If, in addition, the velocity profile has an inflection point with $d^2 [kU_{x0}(y_2) + m_0 U_{z0}(y_2)] / dy_2^2 = 0$ at $y_2 = y_{2c}$, the mechanism of instability becomes essentially inviscid. It was first examined in the pioneering study by Gregory *et al.* (1955) in connection with the stationary vortex pattern on a rotating disk. An even more complicated wave system involves two interacting critical layers (see for example Gajjar, Arebi & Sibanda 1996). For the sake of simplicity we leave aside an in-depth analysis of the velocity fields within the critical layers peculiar to all of these four cases since it does not affect our conclusions of conceptual importance.

4.1. Two-dimensional disturbances with $m_0 = 0$

We begin with the particular case of disturbances introduced by a ribbon the shape of which does not change in the crossflow direction. To this end, m_0 is assumed to be zero with a consequence that $K = k\tau_x$ and $F = k\tau_x \bar{u}_c$. The three-dimensional character of the initial boundary layer with crossflow included proves to be of no significance in these circumstances and the wave system becomes effectively two-dimensional. Accordingly, the expression (3.16) for Q reduces to

$$Q = i^{1/3} \tau_x^{-5/3} (1 - M_\infty^2)^{-1/2} k^{1/3} |k| \quad (4.3)$$

and results given in Ryzhov & Terent'ev (1984, 1986) and Smith (1989) are directly applicable to the analysis of the dispersion relation, with M_∞ and τ_x ruled out by means of an additional affine transformation. In the auxiliary complex Ω -plane all the roots of this relation spring up from the points Ω_{dj} fixed by an equation $d \text{Ai}(\Omega_{dj}) / d\Omega = 0$ ensuing from (4.2) and (4.3) for waves uniformly stretching in the crossflow direction in the limit $k = 0$. Thus, the dispersion-relation roots generating the dispersion curves $\Omega_j(k)$ can be arranged in increasing order of magnitude of the successive negative numbers $\Omega_{dj}, j = 1, 2, 3, \dots$

Using $\Omega_j(k)$ we can easily obtain the dispersion curves $\omega_j(k)$ in the complex ω -plane since $\omega = i^{2/3} \Omega k^{2/3}$ on the strength of (3.13*b*) with $m_0 = 0$ and τ_x eliminated by means of the aforementioned affine transformation. Figure 1 shows five of them labelled 1 to 5; it is worth noting that the curves here do not depend on the value of $\varepsilon_2 D_{(zz)}$. The dispersion curves marked by odd subscripts are drawn as solid lines, the dispersion curves bearing even subscripts are depicted by dotted lines. Each curve consists of two branches located symmetrically about the real axis. Negative

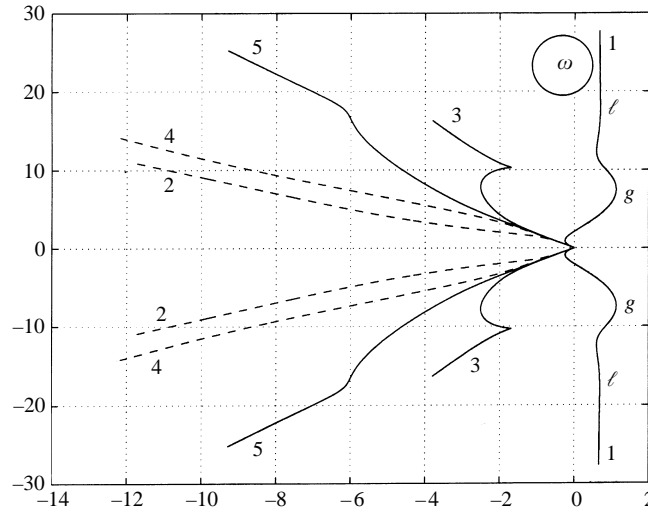


FIGURE 1. Complex frequency plane for the particular case of two-dimensional disturbances.

values of k form a basis for calculating the upper branches of $\omega_1(k), \omega_3(k), \omega_5(k), \dots$, and the lower branches of $\omega_2(k), \omega_4(k), \dots$, on the other hand, positive values of k give rise to the lower branches of $\omega_1(k), \omega_3(k), \omega_5(k), \dots$ and the upper branches of $\omega_2(k), \omega_4(k), \dots$. All the dispersion curves $\omega_j(k)$ stem from the origin $\omega = 0$, which corresponds to $k = 0$, and initially are in the half-plane $\text{Re}(\omega) < 0$. Then both branches of $\omega_1(k)$ make a turn and enter the half-plane $\text{Re}(\omega) > 0$ upon crossing the imaginary axis at the points $\omega = \pm\omega_*i = \pm 2.298i$ when k reaches the critical values $k = \mp k_* = \mp 1.0005$, respectively. These points give neutral oscillations with the amplitude remaining constant in time and space. The two segments of $\omega_1(k)$ from the half-plane $\text{Re}(\omega) < 0$ and the other dispersion curves $\omega_j(k)$ with $j \geq 2$ are associated with stable TS eigenmodes. Both branches of $\omega_1(k)$ with $k_* < |k| < \infty$ positioned in the half-plane $\text{Re}(\omega) > 0$ are responsible for unstable TS eigenmodes. The global and local maxima, labelled g and ℓ respectively, with a local positive minimum of $\text{Re}(\omega_1)$ in between feature each of the branches (Ryzhov & Terent'ev 1984, 1986; Smith 1989). The global maximum attained by $\text{Re}(\omega_1)$ is at the heart of the strong wave-packet formation; the second, barely discernible local maximum of $\text{Re}(\omega_1)$ produces a much weaker subpacket. The modulated oscillatory signals sweep downstream with the group velocities $V_g^* = -d \text{Im} \omega_1(\mp k_g^*)/dk = 4.49$ and $V_\ell^* = -d \text{Im} \omega_1(\mp k_\ell^*)/dk = 8.63$, respectively, where $k_g^* = 2.716$ and $k_\ell^* = 4.346$. Of these two wave packets, the slower one is the most violently developing disturbance propagating in a boundary layer in a linear stage (Ryzhov & Terent'ev 1984, 1986). It is pertinent to note that there exists no wave packet which is capable of moving upstream if $m_0 = 0$.

4.2. Distinctive features of the dispersion curves for three-dimensional waves

The ω -plane drastically changes for values of $m_0 \neq 0$ on account of alterations in the form of the first dispersion curve. It is worth mentioning that the dispersion-relation roots Ω_j now become functions of the streamwise wavenumber k as well as additional parameters $m_0; M_\infty, \varepsilon_2 D_{(zz)}; \tau_x, \tau_z$, the first four of which are actually independent in view of the equality $\tau_x^2 + \tau_z^2 = 1$ connecting the wall-shear-stress components τ_x and τ_z . In what follows, all these parameters are for brevity omitted from the right-hand sides

of the expressions $\Omega = \Omega_j(k, m_0; M_\infty, \varepsilon_2 D_{(zz)}; \tau_x, \tau_z)$ and the corresponding definitions $\omega_j = \omega_j(k, m_0; M_\infty, \varepsilon_2 D_{(zz)}; \tau_x, \tau_z)$ of eigen-frequencies for any $j = 1, 2, \dots$

In order to gain insight into major distinctions of the general case under consideration let us write down an expression

$$\begin{aligned} \omega_1 \sim & -e^{i\pi/2} \frac{k^2 + m_0^2}{K} \left\{ \frac{k^2}{[(1 - M_\infty^2) k^2 + m_0^2]^{1/2}} + \varepsilon_2 m_0^2 D_{(zz)} \right\} \\ & + e^{-i\pi/4} \frac{K^{3/2}}{(k^2 + m_0^2)^{1/2}} \left\{ \frac{k^2}{[(1 - M_\infty^2) k^2 + m_0^2]^{1/2}} + \varepsilon_2 m_0^2 D_{(zz)} \right\}^{-1/2} + \dots \end{aligned} \quad (4.4)$$

determining the asymptotic behaviour of $\omega_1(k)$, as either $k \rightarrow \pm\infty$ or $K \rightarrow \pm 0$, $k \rightarrow k_{lim} = -m_0 \tau_z / \tau_x$. In the former limit, as $k \rightarrow \pm\infty$, we have

$$\operatorname{Re}(\omega_1) \rightarrow \frac{\sqrt{2}}{2} \tau_x^{3/2} (1 - M_\infty^2)^{1/4} > 0 \quad (4.5)$$

no matter what is the value of m_0 in (4.4). Thus, $\operatorname{Re}(\omega_1)$ tends to the same positive constant as it does in the particular case $m_0 = 0$. However in the latter limit $\operatorname{Re}(\omega_1)$ vanishes together with $K \rightarrow \pm 0$ according to

$$\operatorname{Re}(\omega_1) \rightarrow \frac{\sqrt{2}}{2} |K|^{3/2} (k_{lim}^2 + m_0^2)^{-1/2} \left\{ \frac{k_{lim}^2}{[(1 - M_\infty^2) k_{lim}^2 + m_0^2]^{1/2}} + \varepsilon_2 m_0^2 D_{(zz)} \right\}^{-1/2}. \quad (4.6)$$

This implies, in effect, that each of the branches of the first dispersion curve has two different asymptotes stretching to infinity in the lower and the upper half-planes of the complex ω -plane. Both asymptotes are parallel to the imaginary axis and spaced $(\sqrt{2}/2) \tau_x^{3/2} (1 - M_\infty^2)^{1/2}$ apart.

As a consequence, another distinction in the shape of $\omega_1(k)$ arises in the vicinity of the origin. A typical example of a domain centred about the origin is drawn in figure 2 on an enlarged scale for m_0 as small as 0.1. The two branches of the first dispersion curve are seen to become separated, and what is more neither of them meets the real axis. A small positive peak of $\operatorname{Re}(\omega_1)$, labelled d , occurs on each of the branches before they approach the imaginary axis as $K \rightarrow \pm 0$. These peaks grow in magnitude with m_0 exceeding 0.1 and become responsible for the formation of additional weak wave packets as compared to the particular case $m_0 = 0$ where they are lacking.† With the above results at hand, the behaviour of $\omega_1(k)$ for small m_0 in the whole complex ω -plane can be roughly deliniated in the following way. The lower branch, starting from $\operatorname{Im}(\omega_1) \rightarrow -\infty$ and the asymptotic value of $\operatorname{Re}(\omega_1)$ given in (4.5) as $k \rightarrow \infty$, first climbs steeply up, then makes a turn not far from the origin and goes downwards to terminate in (4.6) with $K \rightarrow 0$. The upper branch, springing up symmetrically from $\operatorname{Im}(\omega_1) \rightarrow \infty$ and the same asymptotic value (4.5) of $\operatorname{Re}(\omega_1)$ as $k \rightarrow -\infty$, stops short of reaching the real axis; upon making a turn it proceeds upwards to end in (4.6) with $K \rightarrow -0$. Thus, each branch consists of two segments connected in a single curve as shown in figure 2. The left-hand segments bearing weak positive peaks of $\operatorname{Re}(\omega_1)$ are the salient property of the general case $m_0 \neq 0$. It is just

† The computation points also to the existence of two more tiny peaks of $\operatorname{Re}(\omega_1)$, one on the lower branch and the other on the upper branch. Both tiny peaks are barely discernible in figure 2 due to insufficient resolution and play no part in the analysis below.

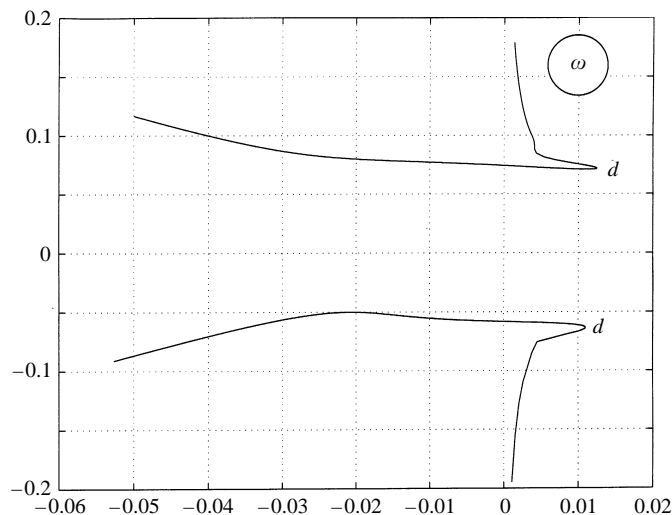


FIGURE 2. The first dispersion curve in the complex frequency plane for $m_0 = 0.1$. Two pairs of segments make up separate branches above and below the real axis.

these segments of the first dispersion curve that lead to the excitation of a special mode of disturbances peculiar solely to three-dimensional boundary layers.†

In more detail the form of the right-hand segments for small m_0 can be found from the computation. With $m_0 \leq 0.1$, the right-hand segments are almost mirror images of each other and bear a certain resemblance to both branches of the first dispersion curve in the particular case $m_0 = 0$ of figure 1. The global and local maxima of $\text{Re}(\omega_1)$ which feature in each of the right-hand segments are similar to the corresponding extrema labelled g and ℓ in that figure. However the resemblance is impaired in the vicinity of the origin. Unlike the particular case $m_0 = 0$, each local negative minimum of $\text{Re}(\omega_1)$ is situated between two points on the imaginary axis giving rise to neutral oscillations with different frequencies. Since the points, where the lower and upper branches of $\omega_1(k)$ intersect the imaginary axis, are placed asymmetrically about the real axis there exist four different values of the neutral frequency. Figure 3 is a plot of all neutral frequencies $\omega_* = \omega_*(m_{0*})$ against the corresponding values $m_0 = m_{0*}$ of the crossflow wavenumber. Damped eigenmodes fall within two shaded domains. Neutral oscillations cease to exist first on the upper branch of the first dispersion curve and then on the lower branch.

The dispersion curves $\omega_j(k)$ with $j = 2, 3, \dots$, do not suffer similar drastic distortions. In the auxiliary complex Ω -plane the corresponding dispersion-relation roots originate, as before, from the points Ω_{dj} specified through $d\text{Ai}(\Omega_{dj})/dY = 0$. These trajectories have their other ends at the points $\Omega_{Ij}^{(\pm)}$ fixed by means of the complex-conjugate roots of an equation $I(\Omega_{Ij}^{(\pm)}) = 0$ where an improper integral $I(\Omega)$ is defined in (3.15b). The points $\Omega_{Ij}^{(\pm)}$ are located in a finite part of the Ω -plane. Hence it

† An analogous spatially damped mode has been briefly mentioned by Mack (1985) and Balakumar & Malik (1990) in connection with rotating-disk flow and exploited by Lingwood (1995) to prove the absolutely unstable character of this motion. The spatially damped mode persists in the framework of an inviscid approach.

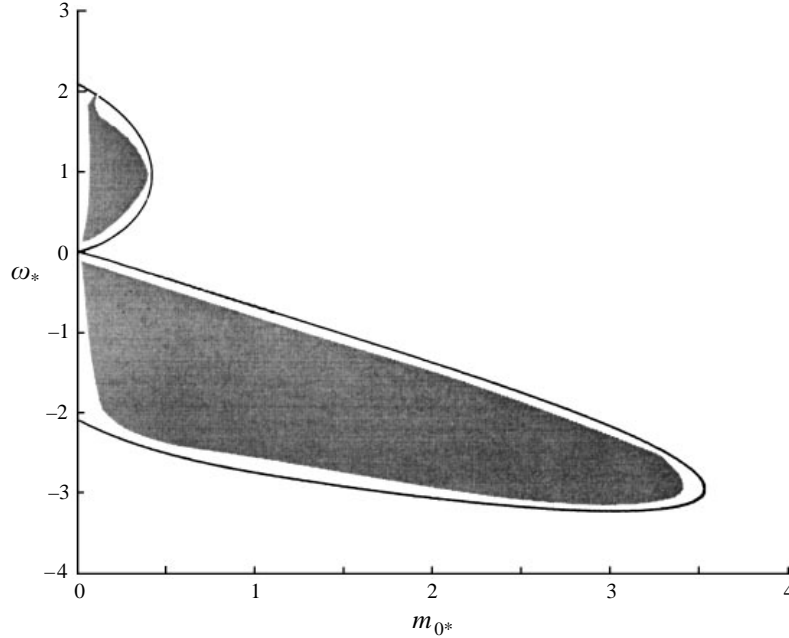


FIGURE 3. Neutral oscillation frequency as a function of the spanwise wavenumber. Two critical values $m_0 = m_0^{(1)} = 1.8$ and $m_0 = m_0^{(2)} = 3.5$ are obtainable with $\omega_0 = 3$.

follows that

$$\Phi \rightarrow \frac{d \text{Ai}(\Omega_{Ij}^{(\pm)}) / dY}{\text{Ai}(\Omega_{Ij}^{(\pm)}) (\Omega_{Ij}^{(\pm)} - \Omega)} \quad \text{as } \Omega \rightarrow \Omega_{Ij}^{(\pm)},$$

and we arrive at an asymptotic expansion

$$\omega_j \sim e^{i\pi/3} K^{2/3} \Omega_{Ij}^{(\pm)} - e^{i\pi/6} \frac{K^{7/3} d \text{Ai}(\Omega_{Ij}^{(\pm)}) / dY}{\text{Ai}(\Omega_{Ij}^{(\pm)}) (k^2 + m_0^2)} \left\{ \frac{k^2}{[(1 - M_\infty^2) k^2 + m_0^2]^{1/2}} + \varepsilon_2 m_0^2 D_{(zz)} \right\}^{-1} + \dots \quad (4.7)$$

which holds in both limiting cases as $k \rightarrow \pm\infty$ or $K \rightarrow \pm 0$, $k \rightarrow k_{lim} = -m_0 \tau_z / \tau_x$. When passing to either of these limits, the second term on the right-hand side of (4.7) gets much smaller in magnitude than the first term and may be disregarded. As a result, the dispersion curves $\omega_j(k)$ with $j = 2, 3, \dots$, preserve their topological forms portrayed in figure 1 for $m_0 = 0$.

The location of these dispersion curves in the left half-plane of the complex ω -plane is rigorously justified using a line of reasoning developed in the general analysis by Ryzhov & Terent'ev (1986, 1991) for $\varepsilon_2 = 0$. With both wavenumbers taking arbitrary real values, the auxiliary complex variable Ω has the aforementioned trajectories arising from the points Ω_{dj} . Variations of Ω within any particular trajectory depending only on $j = 2, 3, \dots$, are allowed in both directions. The change of the direction marks the occurrence of a turning point leading to non-monotonic behaviour of Ω . As applied to the problem under consideration the situation also simplifies because the spanwise wavenumber m_0 is kept constant. Let now ε_2 be non-zero. In view of (3.16),

an additional term proportional to $\varepsilon_2 m_0^2 D_{(zz)}$ enters the right-hand side Q of the dispersion relation (4.2). Although the magnitude of Q changes, its argument remains intact. As we may conclude herefrom, the trajectories in the auxiliary complex Ω -plane preserve their forms notwithstanding the fact that the turning points become shifted to new positions. Since $\omega = i^{2/3} \Omega K^{2/3}$ if $m_0 \neq 0$, all the dispersion curves $\omega_j(k)$ with $j = 2, 3, \dots$, lie in the left half-plane giving rise to stable eigenmodes. The first dispersion curve solely brings about unstable oscillations. They are induced by those portions of the curve which are positioned in the right half-plane of the complex ω -plane and incorporate the aforementioned left segments with two additional small positive peaks of $\text{Re}(\omega_1)$.

4.3. Dependence on the spanwise wavenumber

Distortions in the shape of $\omega_1(k)$ which have surfaced already in figure 2 get much larger with values of m_0 continuously increasing from $m_0 = 0.1$. There are four distinctive ranges of the crossflow wavenumber specified by the following inequalities: I, $0 < m_0 < 2$; II, $2 < m_0 < 5$; III, $5 < m_0 < 7$; IV, $m_0 > 7$.

Figure 4 shown for $m_0 = 1$ presents the complex ω -plane typical of the first range. Asymmetry in the form of two branches of $\omega_1(k)$ and their separation become clear cut even on a smaller scale. Nevertheless, as with values of m_0 only slightly greater than zero, the lower branch of $\omega_1(k)$ where $K > 0$ has a short portion with a local negative minimum of $\text{Re}(\omega_1)$ in the left half-plane of the complex ω -plane. Oscillations associated with this portion are stable except for the end points which lie on the imaginary axis and give rise to neutral disturbances with two different frequencies. If the motion along the right-hand segment of $\omega_1(k)$ starts from the point at infinity, we pass through a local maximum, then a local positive minimum and finally the global maximum of $\text{Re}(\omega_1)$ before reaching the first neutral point with the larger frequency of eigen-oscillations. As in figure 1, the global and local maxima are labelled g and ℓ , respectively; similar notations are used below. The magnitude of the global maximum grows with m_0 increasing in the first range. A small positive peak of $\text{Re}(\omega_1)$ of the type d already known from figure 2 rapidly develops behind the second neutral point with a lesser value of the eigen-frequency when we proceed downwards along the left-hand segment of $\omega_1(k)$ to the point $\text{Im}(\omega_1) \rightarrow -\infty$, $\text{Re}(\omega_1) \rightarrow 0$ as $K \rightarrow 0$.[†] On the other hand, the upper branch of $\omega_1(k)$ where $K \rightarrow 0$ lies entirely in the right half-plane of the complex ω -plane. In accord with figure 3, there is no neutral point on this branch, therefore it contributes only to unstable oscillations. However the magnitude of the global maximum of $\text{Re}(\omega_1)$ on the right-hand segment of the upper branch strongly decreases in the first range with m_0 increasing and becomes half the size of the corresponding global maximum attained on the same segment of the lower branch. As a consequence, the amplitude of periodic wavetrains and especially modulated wave packets related to the upper branch of $\omega_1(k)$ must be far smaller than analogous lower-branch disturbances. One more distinction between the two branches of the first dispersion curve is in the fact that the aforementioned small positive peak of $\text{Re}(\omega_1)$ on the left-hand segment of the lower branch disappears from the left-hand segment of the upper branch.

Figure 5 demonstrates the evolution of the tendencies described above. A value of $m_0 = 3$ chosen here can be considered as a characteristic one for the second range $2 < m_0 < 5$ of the crossflow wavenumbers. There still exists a portion of the lower

[†] One more tiny positive peak of $\text{Re}(\omega_1)$ can be revealed in the left-hand segment using an enlarged scale.

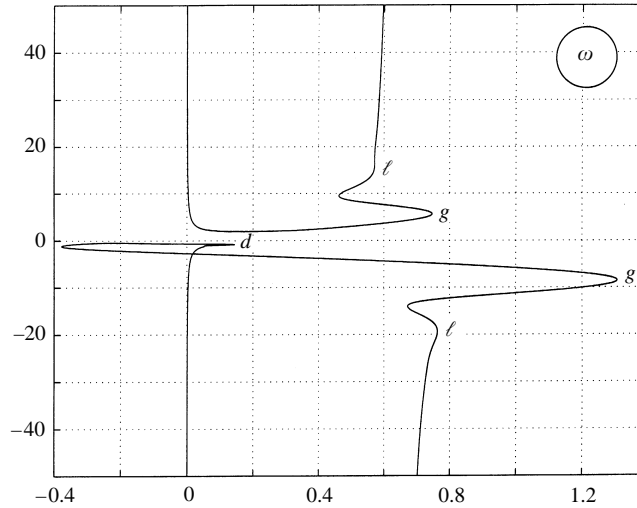


FIGURE 4. The first dispersion curve in the complex frequency plane for $m_0 = 1$. Two branches are seen to become dissimilar.

branch of $\omega_1(k)$ which is situated in the left half-plane of the complex ω -plane with its end points on the imaginary axis. Thus, neutral oscillations persist and can have two different frequencies. However, this portion becomes shorter and bears a weaker local negative minimum of $\text{Re}(\omega_1)$. On the other hand, the magnitude of the global and local maxima of $\text{Re}(\omega_1)$ on the right-hand segment of the lower branch continues to grow with m_0 increasing in the second range. The initially small positive peak d of $\text{Re}(\omega_1)$, occurring behind the second neutral point when we move downwards along the left-hand segment of the lower branch to the point $\text{Im}(\omega_1) \rightarrow -\infty$, $\text{Re}(\omega_1) \rightarrow 0$ as $K \rightarrow 0$, strongly amplifies as well and amounts to up to one third of the global maximum and exceeds one half of the local maximum despite the growing magnitude of these latter.† Both the global and local maxima fade away from the right-hand segment of the upper branch owing to monotonic variations of $\text{Re}(\omega_1)$ provided that $K < 0$. The two branches of the first dispersion curve are found to be dissimilar.

A value $m_0 = 5$ is taken in figure 6 to illustrate the end of the second range and the beginning of the third range extending up to $m_0 = 7$. Referring to this figure, dissimilarities between the two branches making up $\omega_1(k)$ are somewhat smoothed out owing to the fact that the lower branch continues also in the right half-plane of the complex ω -plane without touching the imaginary axis. Thus, both branches of the first dispersion curve induce unstable oscillations, whereas neutral disturbances cease to be a part of the perturbed motion. The global maximum of $\text{Re}(\omega_1)$ on the right-hand segment of the lower branch is at its highest just before the crossflow wavenumber attains a value $m_0 = 5$. Hence the magnitude of the global maximum starts declining with m_0 increasing in the third range. On the other hand, the local maximum of $\text{Re}(\omega_1)$ is highest here. Two kinks barely discernible on the left-hand segment of the lower branch mark the location of additional tiny local maxima. One of them is nothing but a degenerate form of the small peak d of $\text{Re}(\omega_1)$ which starts to rapidly develop in the first range of m_0 (figure 4) and becomes fairly strong in

† A scarcely perceptible kink is in fact an indication to the existence of another tiny peak of $\text{Re}(\omega_1)$.

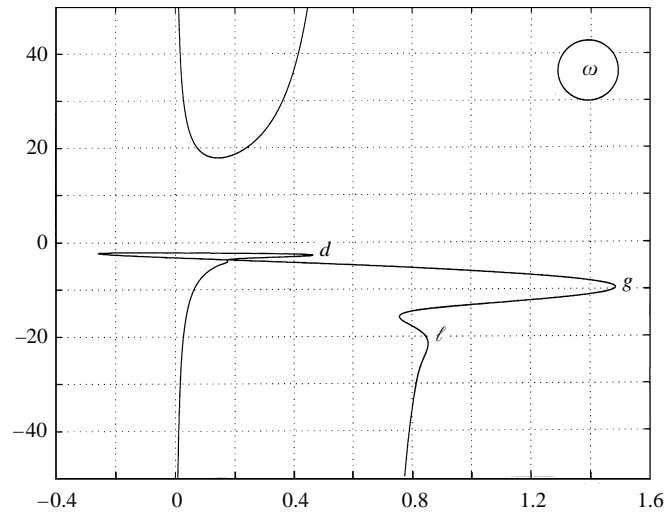


FIGURE 5. The first dispersion curve in the complex frequency plane for $m_0 = 3$. A strong positive peak of $\text{Re}(\omega_1)$ develops on the left-hand segment of the lower branch.

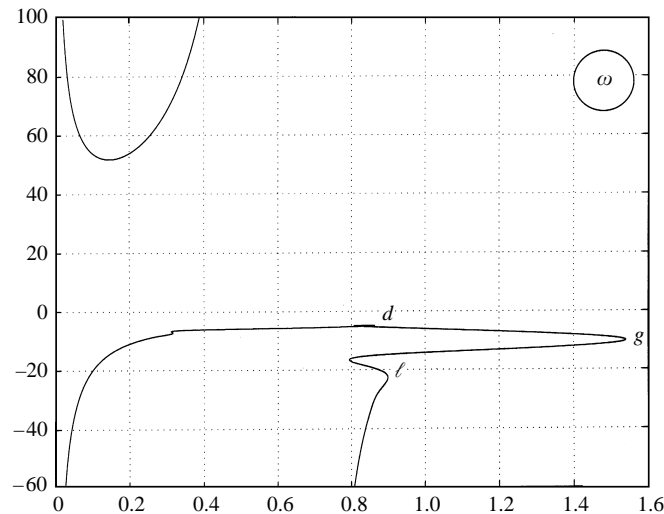


FIGURE 6. The first dispersion curve in the complex frequency plane for $m_0 = 5$. A positive peak of $\text{Re}(\omega_1)$ becomes a tiny kink on the left-hand segment of the lower branch.

the second range (figure 5). The upper branch of the first dispersion curve preserves basically the same shape as that portrayed in figure 5.

Figure 7 drawn for $m_0 = 7$ illustrates the end of the third range and the beginning of the fourth range extending beyond this value of the crossflow wavenumber. The characteristic property of the first dispersion curve under consideration is that the magnitude of the global maximum of $\text{Re}(\omega_1)$ on the right-hand segment of its lower branch significantly falls whereas the neighbouring local maximum remains approximately at the same level as in figure 6. The two extrema become closer to each other. As figure 8 demonstrates, they merge; as a consequence, a single maximum occurs when m_0 is as large as 8. The magnitude of the single maximum declines with

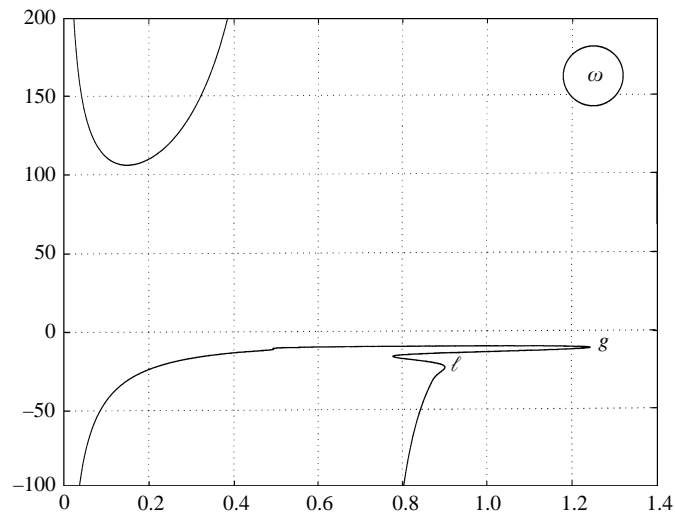


FIGURE 7. The first dispersion curve in the complex frequency plane for $m_0 = 7$. A global maximum of $\text{Re}(\omega_1)$ on the right-hand segment of the lower branch gets smaller.

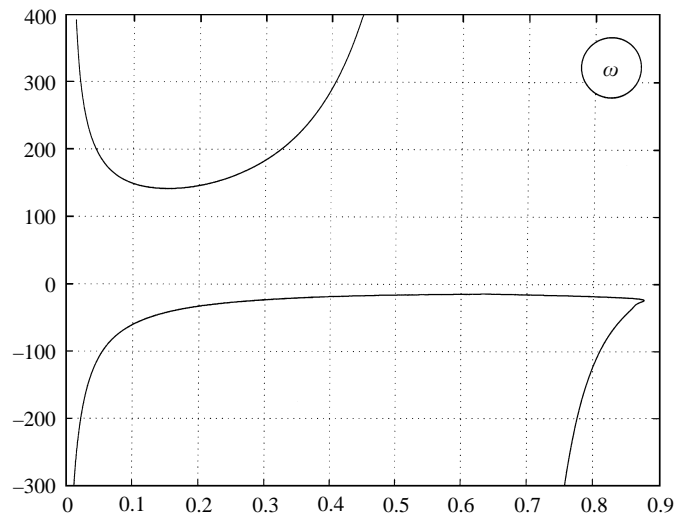


FIGURE 8. The first dispersion curve in the complex frequency plane for $m_0 = 8$. The global and local maxima of $\text{Re}(\omega_1)$ on the right-hand segment of the lower branch merge together.

m_0 increasing in the fourth range $m_0 > 7$. For this reason, unstable waves with large values of the crossflow wavenumber amplify slower in time compared to disturbances from the first three ranges of m_0 . Amplification in space requires a consideration of the associated change in group velocities given below.

4.4. Extremal points of $\text{Re}(\omega_1)$

As is known (see for instance Landau & Lifshitz 1959), positive maxima attained by the real part of the complex frequency result in the wave-packet formation in any viscous shear flow. This property was exploited by Ryzhov & Terent'ev (1984, 1986) to compute the strong amplification of modulated signals in the Blasius boundary layer on a flat plate. Therefore, let us trace the evolution of the global and local maxima of

$\text{Re}(\omega_1)$, in relation to the spanwise wavenumber m_0 , in a three-dimensional boundary layer with crossflow. Our analysis will be confined to the lower branch of $\omega_1(k)$ for it has greater values of $\text{Re}(\omega_1)$ at the extremal points in question compared to the corresponding values characteristic of the upper branch.

Let $\max_g[\text{Re}(\omega_1)]$ and $\max_\ell[\text{Re}(\omega_1)]$ be the magnitudes of $\text{Re}(\omega_1)$ evaluated at those positions where this function takes on, respectively, its global and local maximal values on the right-hand segment of the lower branch. The magnitude of the positive peak of $\text{Re}(\omega_1)$ clearly observable in figures 4 and 5 on the left-hand segment is designated by $\max_d[\text{Re}(\omega_1)]$. Since $d\text{Re}(\omega_1)/dk = 0$ at the points mentioned we may introduce the group velocities V_g^* , V_ℓ^* and V_d^* defined through $V^* = -d\text{Im}(\omega_1)/dk$ and labelled with the same subscripts g , ℓ and d . Variations of $\max_g[\text{Re}(\omega_1)]$ with m_0 are drawn in figure 9(a). $\max_g[\text{Re}(\omega_1)]$ is at its highest, $M_g = 1.54$ at the point $m_0 = m_{0g}^* = 4.87$ where $k = k_g^* = 2.23$. Thus, the two-dimensional case specified by $m_0 = 0$ does not provide the largest rate of disturbance amplification. With $m_0 > 6.0$, the magnitude of $\max_g[\text{Re}(\omega_1)]$ drops sharply. The group velocity V_g^* is shown in figure 9(b) to be positive for all m_0 . Upon reaching a maximum within the interval $0 < m_0 < 1$, it falls to a minimum beyond the point $m_0 = 7$ and then begins to increase again. However, $\max_g[\text{Re}(\omega_1)]$ becomes fairly low in this range of the spanwise wavenumber.

The magnitude of $\max_\ell[\text{Re}(\omega_1)]$ presented in figure 10(a) also grows above a value specific to the two-dimensional case with m_0 increasing up to the point $m_0 = m_{0\ell}^* = 6.20$ where $k = k_\ell^* = 3.80$. At this point the local maximum of $\text{Re}(\omega_1)$ is at its highest $M_\ell = 0.91$, which turns out to be nevertheless below the corresponding value of $\max_g[\text{Re}(\omega_1)]$. With m_0 continuing to increase beyond the point $m_0 = m_{0\ell}^*$, $\max_\ell[\text{Re}(\omega_1)]$ tends to decline; however the tendency develops slowly. As a result, the magnitude of $\max_\ell[\text{Re}(\omega_1)]$ overtakes the magnitude of $\max_g[\text{Re}(\omega_1)]$ diminishing much faster and both extrema merge together giving rise to a single maximum of $\text{Re}(\omega_1)$, already known from figure 8. The group velocity V_ℓ^* in figure 10(b) has a maximum within the interval $1 < m_0 < 2$, drops to a minimum beyond the point $m_0 = 8$ and then again shows an increase, remaining positive for all m_0 .

The behaviour of $\max_d[\text{Re}(\omega_1)]$ in figure 11(a) is of our prime concern because this extremum, like the entire left-hand segments of both branches of $\omega_1(k)$, are intrinsic to three-dimensional boundary layers and missing from two-dimensional flows. The magnitude of $\max_d[\text{Re}(\omega_1)]$ monotonically rises from zero with m_0 varying over an interval $0 < m_0 < 5.3$. However, in the first range, $0 < m_0 < 2$, considered above $\max_d[\text{Re}(\omega_1)]$ is too small compared to $\max_g[\text{Re}(\omega_1)]$ and even to $\max_\ell[\text{Re}(\omega_1)]$ evaluated with the same values of m_0 . As was emphasized above, in the second range, $2 < m_0 < 5$, $\max_d[\text{Re}(\omega_1)]$ rapidly builds up and amounts to about one third of $\max_g[\text{Re}(\omega_1)]$ and exceeds one half of $\max_\ell[\text{Re}(\omega_1)]$ at $m_0 = 3$. What is more important, in figure 5 $\max_d[\text{Re}(\omega_1)]$ is seen to stand out sharply against the level of $\text{Re}(\omega_1)$ typical of the adjacent portion of the first dispersion curve. An analogous topological form of $\omega_1(k)$ persists at $m_0 = 3.5$. On the other hand, by the end of the second range the positive peak of $\text{Re}(\omega_1)$ on the left-hand segment of the lower branch turns into a scarcely perceptible kink (figure 6) and therefore becomes of almost no significance in determining the disturbance pattern induced by a ribbon. As figure 11(b) suggests, the group velocity V_d^* associated with the positive peak of $\text{Re}(\omega_1)$ in question proves to be negative for any m_0 from the interval $0 < m_0 < 5.3$ and becomes zero when $m_0 = 5.3$. With this value of m_0 , the tiny kink disappears from the shape of the first dispersion curve. As a consequence V_d^* ceases to exist if $m_0 > 5.3$.

Except for the points with extremal values of $\text{Re}(\omega_1)$, $d\omega_1/dk$ is complex and

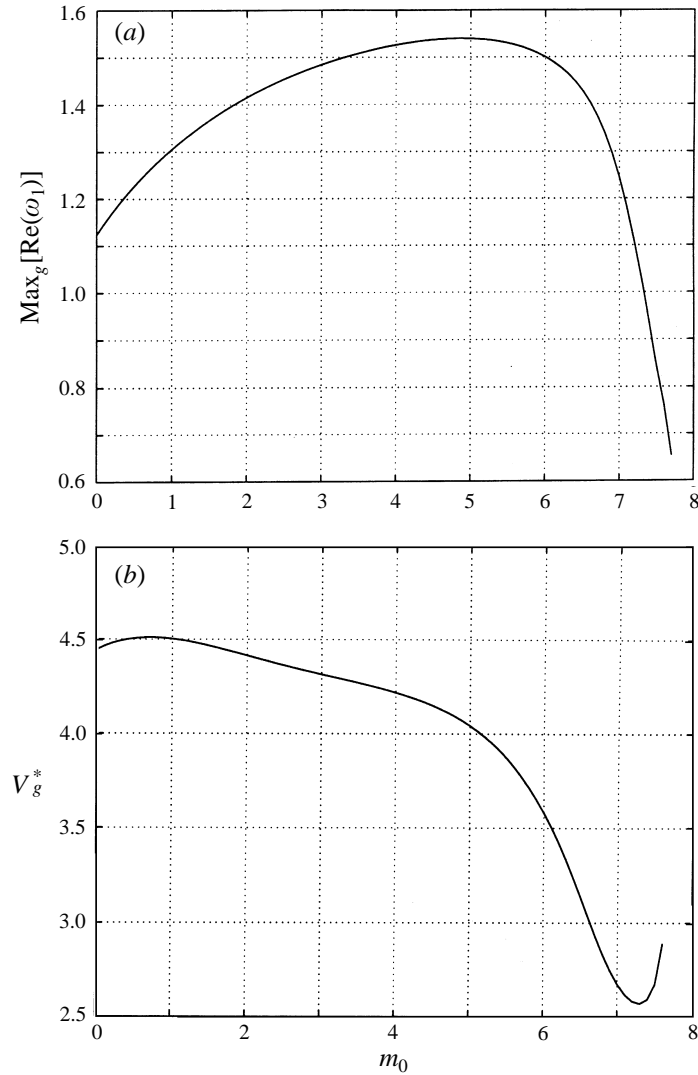


FIGURE 9. (a) Magnitude of the global maximum of $\text{Re}(\omega_1)$ and (b) group velocity corresponding to the global maximum of $\text{Re}(\omega_1)$, on the right-hand segment of the lower branch as a function of the spanwise wavenumber.

then the imaginary part loses its simple meaning. However, the dispersion relation for disturbances in a three-dimensional boundary layer has a specific property. As opposed to positive values of a derivative $V = -d\text{Im}(\omega_1)/dk$ at the points on the right-hand segment, the same derivative takes on negative values along the entire left-hand segment of the lower branch starting from zero at a position where the two segments are connected to make up a single curve. An analogous statement holds true with regard to the upper branch. When applied to the lower and upper branches, the condition $d\text{Im}(\omega_1)/dk = 0$ determines two respective values, $k = k_r^{(-)}(m_0)$ and $k = k_r^{(+)}(m_0)$, of the streamwise wavenumber. Hence $d\text{Im}(\omega_1)/dk < 0$ occurs in a finite range $k_r^{(+)} < k < k_r^{(-)}$ where $\text{Re}(\omega_1) > 0$, rather than being valid locally. Thus, we may expect that both left-hand segments of $\omega_1(k)$ located in the lower as well as upper

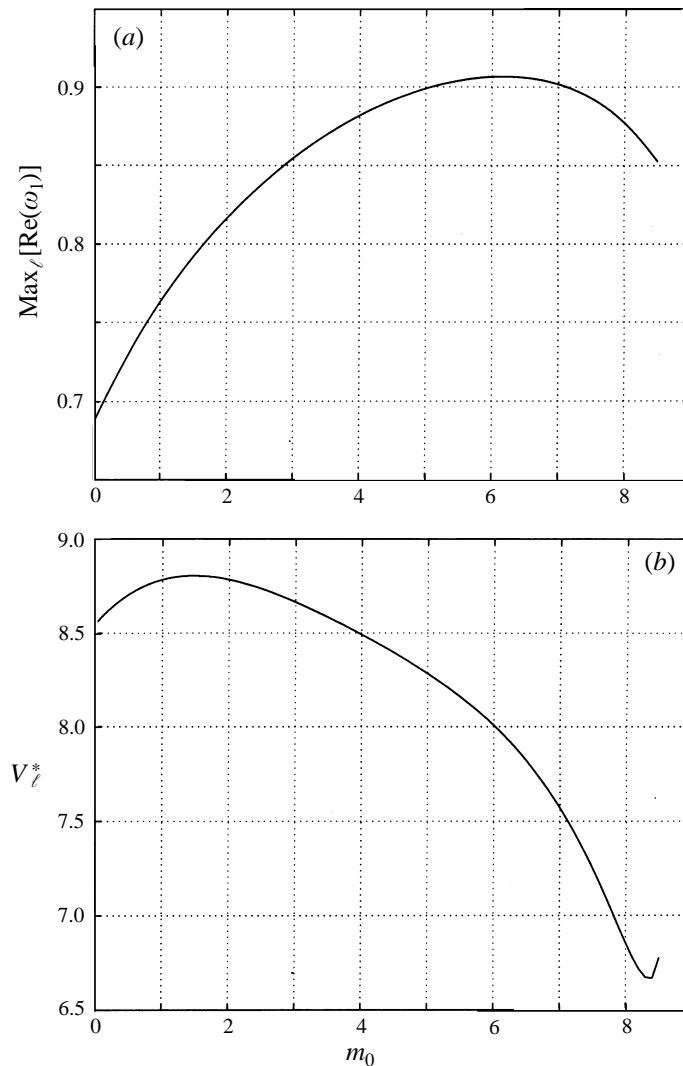


FIGURE 10. (a) Magnitude of the local maximum of $\text{Re}(\omega_1)$ and (b) group velocity corresponding to the local maximum of $\text{Re}(\omega_1)$, on the right-hand segment of the lower branch as a function of the spanwise wavenumber.

half-planes of the complex ω -plane are capable of contributing to the excitation of amplifying modulated disturbances in a region upstream of the ribbon. Should this be the case, the three-dimensional boundary layer would be absolutely unstable in the streamwise direction.

A rigorous treatment to provide support for this view is usually based on a criterion stated by Briggs (1964) and Bers (1975) for unstable two-dimensional wave systems in plasmas. Recently, a pertinent formalism was extended by Brevdo (1991) to the general three-dimensional case and exploited by Lingwood (1995) when analysing the rotating-disk flow. Unlike the above discussion confined to real streamwise wavenumbers, the dispersion relation roots are also traced in the complex k -plane. As applied to the problem in question, a point $k = k_p(m_0)$ of zero $d\text{Im}(\omega_1)/dk$ with positive $\text{Re}(\omega_1)$ is necessary, but in general not sufficient, for streamwise instability to occur. For

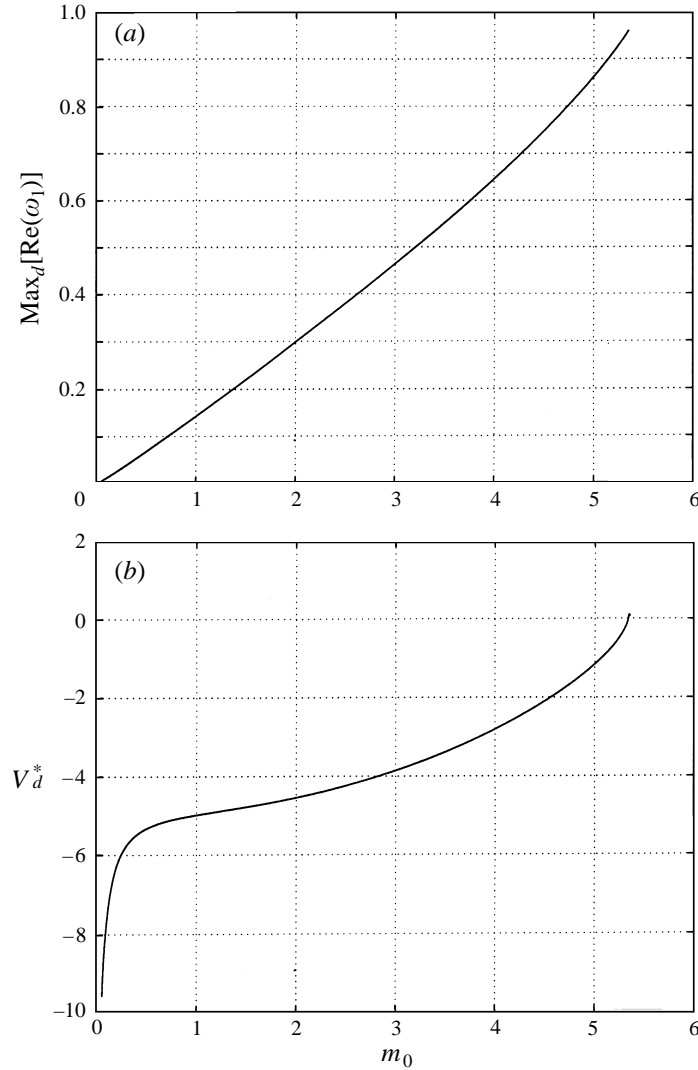


FIGURE 11. (a) Magnitude of the positive peak of $\text{Re}(\omega_1)$ and (b) group velocity corresponding to the positive peak of $\text{Re}(\omega_1)$, on the left-hand segment of the lower branch as a function of the spanwise wavenumber.

this condition to become sufficient, a pinching requirement for two colliding roots of the dispersion relation has to be met. The essence of the additional constraint is as follows: the two roots that coalesce at the point $k = k_p$ in the complex wavenumber plane must originate on the opposite sides of the real axis when $\text{Re}(\omega_1)$ takes on sufficiently large positive values. It is easily seen that the function $\omega_1 = \omega_1(k)$ has a saddle point at $k = k_p$ (Brevdo 1991). Evidently neither $k_r^{(-)}$ nor $k_r^{(+)}$ are the saddle points of $\omega_1(k)$.

Noteworthy are branch points in the complex k -plane. A function on the right-hand side of (3.16) gives rise to three of them, $K = 0$ and $k = \pm i m_0 / (1 - M_\infty^2)^{1/2}$ located on the real and imaginary axis, respectively. Also, infinite sets of branch points emerge from the collision of different spatial branches of the dispersion-relation roots. Their location in the complex auxiliary Ω -plane varies with m_0 . A branch cut is drawn

through each of the points mentioned. In order to remain on the same sheet of a Riemann surface, the branch cuts must be avoided by the colliding roots when checking the pinching requirement. Due to the cut arising from $K = 0$ the behaviour of the spatial branches of the first dispersion curve becomes intricate and strongly depends on a value of the crossflow wavenumber. This is why the approach under discussion does not appear worthy of pursuing further.

The method of steepest descent offers an alternative rigorous approach to evaluating the inverse Laplace–Fourier transform in (3.20) and resolving the issue of absolute instability. A brief discussion of this technique is postponed until the next Section.

5. Pressure variations

With the dispersion-relation properties at hand, we may proceed to working out the excess pressure induced by the ribbon. An explicit expression for its shape $f(x)$ entering (2.9) was of no significance in the general analysis; however in the computation it is convenient to put $f = \pi^{-1/2}\exp(-x^2)$ with a consequence that the corresponding Fourier transform $\hat{f} = \exp(-k^2/4)$. This choice ensures fast decay of \bar{p}_c specified by (3.17) as $k \rightarrow \pm\infty$.

5.1. Asymptotic simplification for large times

Insofar as a continuous part is missing from the ω -spectrum let us expand the inverse Laplace transform entering a relationship for the self-induced pressure p_c into series in residues of the integrand at its poles. Using (3.20) we have

$$J = \int_{\ell-i\infty}^{\ell+i\infty} \frac{\Phi(\Omega)e^{\omega t} d\omega}{(\omega^2 + \omega_0^2)[\Phi(\Omega) - Q(k, m_0; M_\infty, \varepsilon_2 D_{(zz)}; \tau_x, \tau_z)]} = \frac{\pi}{\omega_0} J_0 + 2\pi i J_1, \quad (5.1a)$$

$$J_0 = e^{i\omega_0 t} \frac{\Phi(\Omega_0)}{\Phi(\Omega_0) - Q(k, m_0; M_\infty, \varepsilon_2 D_{(zz)}; \tau_x, \tau_z)} - e^{-\omega_0 t} \frac{\Phi(-\Omega_0)}{\Phi(-\Omega_0) - Q(k, m_0; M_\infty, \varepsilon_2 D_{(zz)}; \tau_x, \tau_z)}, \quad (5.1b)$$

$$J_1 = \sum_{j=1}^{\infty} \frac{1}{\omega_j^2(k) + \omega_0^2} e^{\omega_j(k)t} \frac{\Phi(\Omega_j)}{\partial \Phi(\Omega_j)/\partial \omega}, \quad (5.1c)$$

where $\Omega_0 = i^{1/3}\omega_0 K^{-2/3}$ and, in keeping with the above abbreviations, $\omega_j(k) = \omega_j(k, m_0; M_\infty, \varepsilon_2 D_{(zz)}; \tau_x, \tau_z) = i^{2/3}K^{2/3}\Omega_j(k, m_0; M_\infty, \varepsilon_2 D_{(zz)}; \tau_x, \tau_z)$, $j = 1, 2, \dots$. The first term J_0 in (5.1a) derives from the two roots (4.1) and is periodic in time. The second term J_1 consists of contributions associated with the roots $\omega_j(k)$, $j = 1, 2, \dots$, of the dispersion relation. As was proved in the preceding Section, only the first root $\omega_1(k)$ gives rise to unstable oscillations whereas all the other eigenmodes caused by the roots $\omega_j(k)$ with $j = 2, 3, \dots$, damp out with time both upstream and downstream of the ribbon. Therefore, in an asymptotic representation for J_1 we may confine ourselves to the leading-order approximation and write

$$J_1 \sim \frac{1}{\omega_1^2(k) + \omega_0^2} e^{\omega_1(k)t} \frac{\Phi(\Omega_1)}{\partial \Phi(\Omega_1)/\partial \omega} \quad \text{for large } t, \quad (5.2)$$

in place of (5.1c). It is pertinent to note at this point that the determination of unstable disturbances and neglect of decaying eigenmodes leaves aside transient dynamics in

favour of the asymptotic state (for a discussion of a transient stage in the wave-pattern development see Benny & Gustavsson 1981 and Criminale & Drazin 1990 and references therein).

With the simplifications achieved, the self-induced pressure becomes

$$p_c = p_{c0} + p_{c1}. \quad (5.3)$$

In view of (5.1*b*), the time-periodic part p_{c0} of oscillations is fixed by

$$p_{c0} = -\frac{i}{4\pi} \int_{-\infty}^{\infty} dk e^{ikx-k^2/4} \left\{ k^2 [(1 - M_\infty^2) k^2 + m_0^2]^{-1/2} + \varepsilon_2 m_0^2 D_{(zz)} \right\} \\ \times \left[e^{-i\omega_0 t} \frac{\Phi(-\Omega_0)}{\Phi(-\Omega_0) - Q(k, m_0)} - e^{i\omega_0 t} \frac{\Phi(\Omega_0)}{\Phi(\Omega_0) - Q(k, m_0)} \right] \quad (5.4)$$

with parameters $M_\infty, \varepsilon_2 D_{(zz)}$; τ_x, τ_z omitted when indicating the arguments of Q . On the strength of (5.2) and a relation $d\Phi/d\Omega = \text{Ai}(\Omega)[\Omega + \Phi(\Omega)]I^{-1}(\Omega)$, the second term p_{c1} in (5.3) that gives the exponentially amplifying disturbances in time and space can, to leading order, be reduced to

$$p_{c1} = -\frac{i^{2/3}\omega_0}{2\pi} \int_{-\infty}^{\infty} dk e^{\omega_1(k)t+ikx-k^2/4} \left\{ k^2 [(1 - M_\infty^2) k^2 + m_0^2]^{-1/2} + \varepsilon_2 m_0^2 D_{(zz)} \right\} \\ \times \frac{K^{2/3} d \text{Ai}(\Omega_1)/dY}{[\omega_1^2(k) + \omega_0^2] \text{Ai}(\Omega_1)[\Omega_1 + \Phi(\Omega_1)]} \quad \text{for large } t. \quad (5.5)$$

Both contributions p_{c0} and p_{c1} to the self-induced pressure variations are expressed through single integrals making the final stage of analysis amenable to treatment with the steepest descent method. Let us dwell briefly on the main concepts underlying this standard technique as applied to evaluating exponentially growing disturbances. The existence of saddle points of the complex phase function $\varphi = \omega_1(k, m_0) + iVk$, $V = x/t$ entering the exponent of the integrand in (5.5) is central to the steepest descent method; their coordinates $k = k_s(m_0; V)$ come from

$$\frac{d\omega_1}{dk} + iV = 0.$$

Here we may put $V \rightarrow 0$ in determining the large-time response for any finite $x=\text{const}$ to resolve the issue of streamwise absolute instability. However, our interest is in the whole wave pattern, both downstream and upstream of the ribbon, rather than in the behaviour of oscillations in the immediate vicinity of it. A complete set of saddle points is needed to compute the pressure distribution from (5.5) along an arbitrary ray $x/t = \text{const}$. It should be recognized that a saddle point $k = k_s$ contributes to instabilities if the original integration path along the real axis can be continuously deformed into a steepest descent contour through this particular point. The existence of k_s by itself does not imply at all that such a contour is obtainable for any m_0 and V . Thus, the properties of the phase function $\varphi = \varphi(k, m_0; V)$ in the entire complex k -plane should be investigated for feasibility of drawing the steepest descent contour through each saddle point. Notice that in addition to the aforementioned branch points at $K = 0$ and $k = \pm i m_0 / (1 - M_\infty^2)^{1/2}$, three sets of branch points result from the coalescence of ω_1 with the other roots ω_j , $j = 2, 3, \dots$, of the dispersion relation. In the auxiliary complex Ω -plane all the points where any two temporal branches coalesce are fixed by $d\Phi/d\Omega = 0$. For $d\Phi/d\Omega = \text{Ai}(\Omega)[\Omega + \Phi(\Omega)]I^{-1}(\Omega)$, their positions are defined either by the real negative zeros of the Airy function or by the pairs of complex conjugate zeros of a function $\Psi = \Omega + \Phi(\Omega)$. The three sets

of zeros found in the complex Ω -plane give rise to the corresponding sets of branch points in the complex k -plane. A branch cut should be drawn through each of these points. Thus, examining the global topography of the phase function becomes the most tedious part of the analysis.

A complete study for two-dimensional oscillations with $m_0 = 0$ may be found in Ryzhov & Terent'ev (1986). Even in this simplest particular case there are two families of saddle points none of which contributes, in accord with the well-known results, to streamwise absolute instability. With $m_0 \neq 0$ the number of the saddle-point families increases and strongly depends on a value of the crossflow wavenumber. For instance, if $m_0 = 3$ five families come into existence only for the phase function based on the lower branch of the first dispersion curve. However a check upon the feasibility of absolutely unstable disturbances being excited in the streamwise direction of a three-dimensional boundary layer requires $V = 0$. The saddle point of the phase function specified by this condition becomes simultaneously a saddle point of the complex frequency. In examples considered below the original integration path in the Fourier transform (5.5) proves to be continuously deformable into the steepest descent contour through the saddle point of $\omega_1 = \omega_1(k, m_0)$. Thus, we are led to the conclusion that streamwise absolute instability is triggered in response to the initial motion of the ribbon.

The contributions from p_{c0} and p_{c1} were calculated numerically using the FFT algorithm to speed up the computation with real k . Results and their elucidation in terms of the dispersion-relation properties are set forth below. They provide not only the conclusive evidence for streamwise absolute instability but, what is more important, reveal fundamental mechanisms in different regimes of excitation depending on the crossflow wavenumber. In most cases periodic oscillations and rapidly growing wave packets were computed for the same time $t = 10$. This value was found to separate wave packets excited during the initial pulse motion of the ribbon from disturbances continuously fed by its subsequent monochromatic vibrations.

5.2. Periodic oscillations

The distribution of p_{c0} with distance from the vibrating ribbon strongly depends on m_0 . In the particular case $m_0 = 0$, the periodic part under consideration contributes significantly to pressure variations in the vicinity of the external source where a TS wave is formed (Terent'ev 1984). At $t \leq 10$, essentially three-dimensional disturbances with $m_0 \neq 0$ are dominated by wave packets developing from a contribution given by p_{c1} . Under these circumstances periodic oscillations become of less significance.

Critical values m_{0*} of the spanwise wavenumber provoking drastic changes in the pressure distribution are fixed by a requirement that ω_0 should coincide with a frequency ω_* of neutral oscillations, i.e. $\text{Re}(\omega_1) = 0$, $\text{Im}(\omega_1) = \omega_*(m_0) = \pm\omega_0$. As figure 3 shows, there are two critical values $m_0 = m_{0*}^{(1)} = 1.8$ and $m_0 = m_{0*}^{(2)} = 3.5$ of the spanwise wavenumber which correspond to the prescribed neutral frequency $\omega_0 = 3$. Both critical values are determined by the lower branch of the first dispersion curve. In accord with the behaviour of ω_1 in figures 2 and 4–8, no value of m_{0*} comes from the upper branch of this curve. As a result, there exist three distinctive ranges of the spanwise wavenumber specified by the following inequalities: I_p, $0 < m_0 < 1.8$; II_p, $1.8 < m_0 < 3.5$; III_p, $m_0 > 3.5$ provided that $\omega_0 = 3$. Clearly, they have nothing to do with the four characteristic ranges of eigenmodes analysed in §4. The critical values $m_{0*}^{(1)}$ and $m_{0*}^{(2)}$ separating the ranges of periodic oscillations strongly depend on the forcing frequency ω_0 . Besides, it should be kept in mind that $\Omega_0 = i^{1/3}\omega_0 K^{-2/3}$ in the difference $\Phi(\pm\Omega_0) - Q(k, m_0)$ entering the right-hand side of (5.4). When

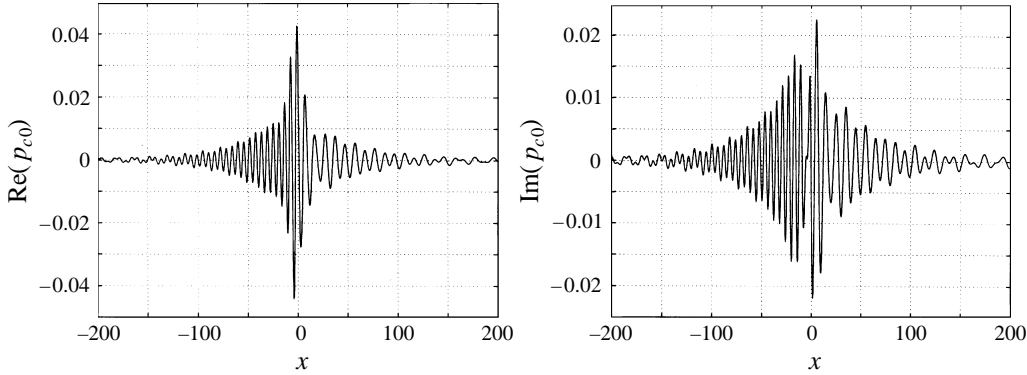


FIGURE 12. Real and imaginary parts of periodic oscillations of the ribbon-induced pressure vs. the streamwise distance; $m_0 = 1.2$; $t = 10$.

$\Phi(\pm\Omega_0) - Q(k, m_0)$ passes through zero, the dispersion relation comes into play in the complex k -plane and can be used to identify the critical values $k_*^{(1)}$ and $k_*^{(2)}$ of the streamwise wavenumber associated with neutral oscillations. The same critical values $m_{0*}^{(1)}$ and $m_{0*}^{(2)}$ of the spanwise wavenumber are readily apparent from the respective conditions $\text{Re}(k_*^{(1)}) = 0$ and $\text{Re}(k_*^{(2)}) = 0$. Damped eigenmodes fall within two shaded domains in figure 3; unstable oscillations are represented by the points which lie outside their boundaries.

A TS wave generated in the particular case $m_0 = 0$ amplifies downstream of the ribbon vibrating with the frequency $\omega_0 = 3$. However in order to evaluate the growth rate with distance, it is necessary to take into account a contribution from p_{c1} becoming dominant in the region $x > 0$ (Terent'ev 1984). An oscillatory tongue conditioned by the TS wave radiation arises in the distribution of p_{c0} with x which decays in the upstream direction (not shown). The pressure variations of the type intrinsic to p_{c0} in the particular case $m_0 = 0$ persist up to the first critical value $m_{0*}^{(1)} = 1.8$. An exception occurs in a narrow interval centred about $m_0 = 1.2$ where oscillations portrayed in figure 12 develop and fade out in both directions, downstream as well as upstream of the ribbon. The excitation of an oscillatory tongue in the region $x > 0$ is easily explainable if allowance is made for the properties of the dispersion relation in the complex k -plane where two roots become close in magnitude and opposite in sign. The root $k_s^{(+)}$ in figure 13 stems from (4.1) where $\omega = i\omega_0 = 3i$. This root is basic to the downstream portion of disturbances, because $\min[\text{Re}(k_s^{(+)})] = 0.07$ achieved at $m_0 = 1.2$ compares in magnitude to the value $\text{Re}(k_1^{(-)}) = -0.04$ taken at the same point by the real part of the first root $k_1^{(-)}$ which derives from (4.1) with $\omega^{(-)} = -i\omega_0 = -3i$. However, $\text{Re}(k_s^{(+)})$ grows very fast beyond the immediate vicinity of $m_0 = 1.2$; therefore the downstream spreading oscillatory motion does not typify the first range of the spanwise wavenumbers.

On the other hand, the oscillatory tongue behind the ribbon becomes a distinctive feature of the disturbance pattern in the second range $1.8 < m_0 < 3.5$. The computation reveals no forced time-periodic oscillations in front of the perturbing source specified by the spanwise wavenumber from this range.

The distribution of p_{c0} with x drastically changes on passing through the second critical value $m_{0*}^{(2)} = 3.5$. The oscillatory tongue behind the ribbon disappears and instead an upstream spreading tail emerges as a dominant property of the disturbance pattern. However the oscillatory motion ceases to exist in space, when the spanwise

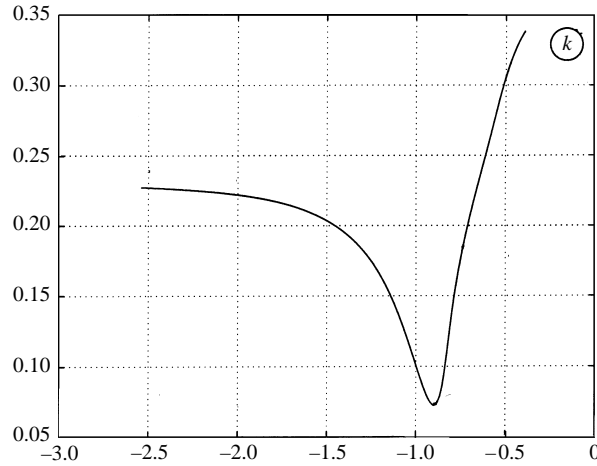


FIGURE 13. The root $k_s^{(+)}$ in the complex wavenumber plane for $\omega_0 = 3$. $\text{Min}[\text{Re}(k_s^{(+)})]$ is achieved with $m_0 = 1.2$.

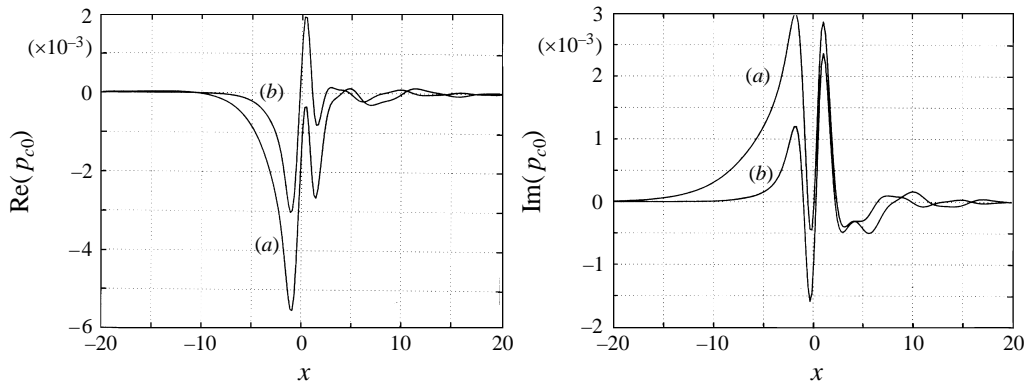


FIGURE 14. Real and imaginary parts of periodic oscillations of the ribbon-induced pressure vs. the streamwise distance; (a) $m_0 = 4$; (b) $m_0 = 4.5$; $t = 10$.

wavenumber falls within the third range $3.5 < m_0$, and very soon gives way to the disturbance of the type exhibited in figure 14 for $m_0 = 4$ and 4.5 . Even smoother variations of p_{c0} are typical of larger values of m_0 . The amplitude of the forced time-periodic oscillations drops with m_0 increasing.

5.3. Downstream-sweeping wave packets with moderate values $0 < m_0 < 7$

Qualitatively, the wave system generated by switching on the perturbing source may be outlined even without evaluating the integral on the right-hand side of (5.5). Conclusions of conceptual significance are easily derivable from the form of the first dispersion curve in the complex ω -plane which has been elucidated in §4. Since the limit (4.5) holds for all four ranges of m_0 as $k \rightarrow \infty$ as well as $k \rightarrow -\infty$, both branches of this curve situated in the lower and upper half-planes make an equal contribution to a long oscillatory tongue in front of downstream-moving disturbances. Pulsations here are given by the application of the Kelvin stationary-phase principle (or the steepest descent technique) on the condition that $x/t \gg 1$. In presenting the final result we confine ourselves to two-dimensional wave packets with $m_0 = 0$ to give an

idea of how the excess pressure develops in the most advanced region of oscillations. In this particular case the leading term of an asymptotic representation reads

$$p_{c1} = \frac{2\omega_0\tau_x^{1/2}}{\pi^{1/2}(1-M_\infty^2)^{1/4}} \exp\left(\frac{\sqrt{2}}{2}\tau_x^{3/2}(1-M_\infty^2)^{1/4}t - \frac{\tau_x^2(1-M_\infty^2)}{16}\frac{x^2}{t^2}\right) \frac{t^{1/2}}{x} \\ \times \sin\left[\frac{\tau_x(1-M_\infty^2)^{1/2}}{4}\frac{x^2}{t} + \frac{\sqrt{2}}{2}\tau_x^{3/2}(1-M_\infty^2)^{1/4}t - \frac{\pi}{4}\right]. \quad (5.6)$$

The oscillatory tongue is similar to that studied in Ryzhov & Terent'ev (1984, 1986) in connection with stability of the Blasius boundary layer. Structurally, the oscillation tongue is determined by the initial pulse-mode stage of switching on the perturbing source. The short-scaled wave pattern in (5.6) specified by $\tau_x(1-M_\infty^2)^{1/2}x^2/(4t)$ ensues from the superposition of the quasi-two-dimensional TS eigenmodes. As regards τ_x and $1-M_\infty^2$, it obeys the conventional triple-deck normalization not included in (2.3a, b). The dependence of the most rapidly sweeping part of disturbances on the spanwise wavenumber makes the pressure distribution far more complicated. Variations in the crossflow direction are accounted for through a multiplier $\text{Re}(e^{im_0z})$ in (3.3) dictated by the shape (2.9) of the ribbon. Note, however, that the oscillatory tongue might be strongly affected by the formation of a critical layer at some distance from the solid surface. This issue is left aside in the present study.

As (5.6) shows, the short-scaled wave motion exponentially amplifies in time at any point in space. We may thus expect that the pressure distribution given in p_{c1} becomes a rapidly growing function of the streamwise coordinate in a transitional-type region next to the oscillatory tongue. This statement can be readily justified by exploiting properties of the first dispersion curve in the complex ω -plane. As figure 4 discloses, the global and local maxima with a local minimum of $\text{Re}(\omega_1)$ in between feature in the right-hand segments of both the lower and upper branches of this curve in the first range $0 < m_0 < 2$ of the spanwise wavenumber. Each maximum gives rise to a wave packet exponentially growing in time and space. However contributions to p_{c1} from the maxima of $\text{Re}(\omega_1)$ are far from being equivalent. The dominant role in exciting vigorous pulsations is played by the global maximum on the lower branch because the magnitude of the corresponding maximum on the upper branch is about 1.7 times less when $m_0 = 1$. Of the same size is the local maximum on the lower branch whereas an analogous maximum on the upper branch tends to decay. The global maximum of $\text{Re}(\omega_1)$ on the upper branch provides an essential contribution to p_{c1} only when m_0 is small enough. If we leave aside this nearly two-dimensional regime, the pulsation pattern consists of the main large-amplitude wave packet moving downstream with the group velocity $V_g^* = V_g^*(m_0)$ presented in figure 9(b) and three subpackets having their intrinsic group velocities. The subpacket deriving from the local maximum on the lower branch of the first dispersion curve sweeps faster with the group velocity $V_\ell^* = V_\ell^*(m_0)$ depicted in figure 10(b). It is located between the oscillatory tongue (5.6) and the main wave packet. With reference to Ryzhov & Terent'ev (1984, 1986) we may anticipate, however, all three weaker subpackets to be indiscernible against the background of vigorous pulsations in the main wave packet. Figure 15 computed for $m_0 = 1$ confirms this claim, showing a system of oscillation cycles in the form of a single highly-modulated disturbance. The group velocity of the disturbance is close to $V_g^*(1) = 4.5$ in figure 9(b).

The wave system downstream of the ribbon simplifies in the second range $2 < m_0 < 5$ of the spanwise wavenumber. According to figure 5 drawn for a typical value

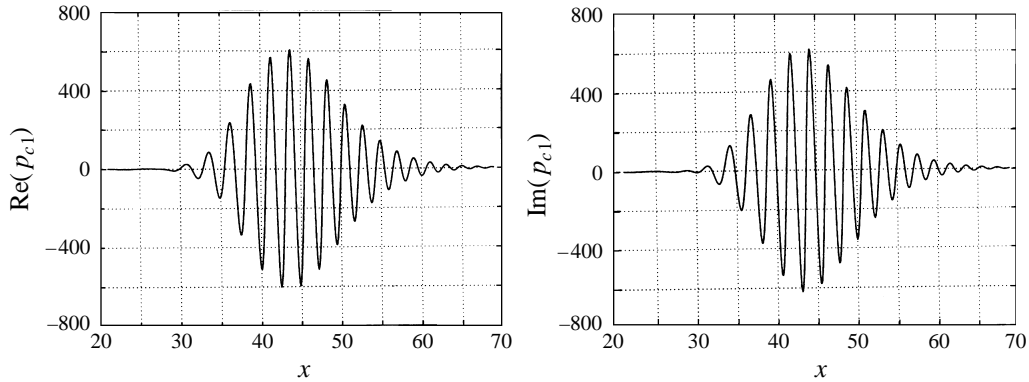


FIGURE 15. Ribbon-induced pressure distributions vs. the streamwise coordinate in the downstream-sweeping wave packet for $m_0 = 1$; $t = 10$.

$m_0 = 3$, no subpacket can be associated with the upper branch of the first dispersion curve insofar as all the extrema of $\text{Re}(\omega_1)$ are missing from its right-hand segment. The same statement holds true for the third range $5 < m_0 < 7$ exemplified by the plots in figures 6 and 7 where the global and local maxima of $\text{Re}(\omega_1)$ feature only the right-hand segment of the lower branch. Figure 16 exhibits a single highly-modulated disturbance for a value $m_0 = 5$ separating the second and the third ranges. The disturbance is actually driven by the global maximum. Contributions to central large-amplitude cycles from the other parts of the first dispersion curve, including the local maximum of $\text{Re}(\omega_1)$ on its lower branch, are small. At $t = 10$, the oscillation swing in the wave system defined by $m_0 = 5$ is about ten times greater than in the wave packet in figure 15 for $m_0 = 1$. The most rapidly growing disturbances originate in the computation from the ribbon with $4.5 < m_0 < 5$. The reason behind the strongest amplification of the wave packets having values of m_0 within this particular interval of the spanwise wavenumber becomes evident from inspection of figure 9(a) where $\max_g[\text{Re}(\omega_1)]$ is at its highest at $m_0 = m_{0g}^* = 4.87$ and then sharply drops with the spanwise wavenumber approaching the end-point $m_0 = 7$ of the third interval. The disturbance in figure 16 sweeps downstream with the group velocity $V_g^*(5) = 4.0$ being nearly equal to that in figure 9(b). In the third range of the crossflow wavenumber the computed group velocity $V_g^* = V_g^*(m_0)$ monotonically diminishes to become as low as $V_g^*(7) = 2.6$. Figure 9(b) predicts the same behaviour.

5.4. Upstream-advancing wave packets

The existence of highly modulated signals capable of moving against the oncoming stream is also directly inferable from the form of the first dispersion curve in the complex ω -plane. As has been elucidated in §4, a small positive peak of $\text{Re}(\omega_1)$ can develop on the left-hand segment of the lower branch behind the second neutral point. Figure 4 typifies the first range $0 < m_0 < 2$ of the spanwise wavenumber. This peak is strongly magnified in the second range $2 < m_0 < 5$. Figure 5 gives evidence for a characteristic case $m_0 = 3$ when $\max_d[\text{Re}(\omega_1)]$ amounts to one-third of the global maximum and exceeds one-half of the local maximum on the right-hand segment despite the large magnitudes of both $\max_g[\text{Re}(\omega_1)]$ and $\max_l[\text{Re}(\omega_1)]$. In fact there is one more tiny peak (or at least scarcely perceptible kink) of $\text{Re}(\omega_1)$ in the shape of the left-hand segment of the lower branch, but the occurrence of additional minute extrema does not play any role in building up the overall wave pattern.

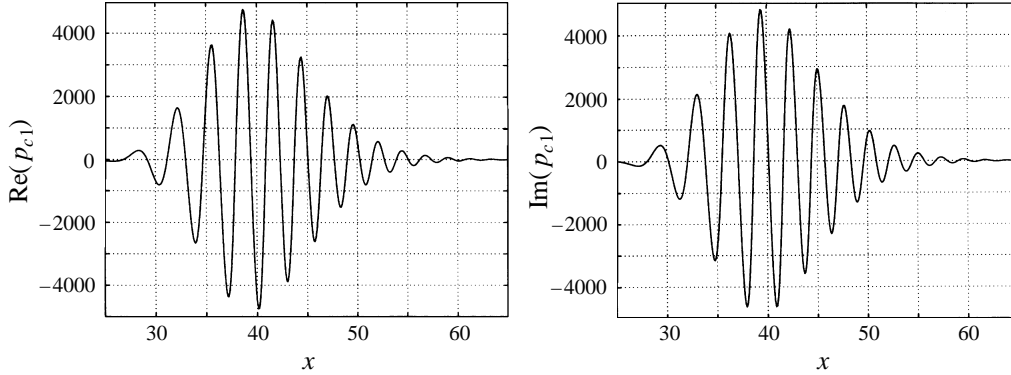


FIGURE 16. Ribbon-induced pressure distributions vs. the streamwise coordinate in the downstream-sweeping wave packet for $m_0 = 5$; $t = 10$.

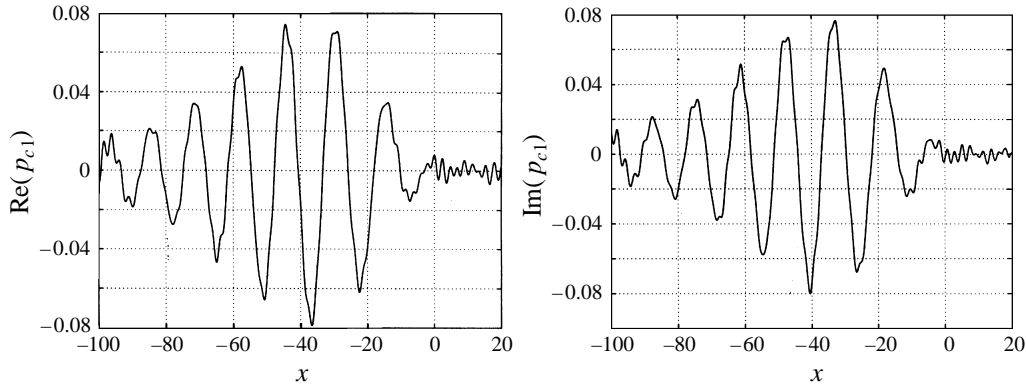


FIGURE 17. Ribbon-induced pressure distributions vs. the streamwise coordinate in the upstream-advancing wave packet for $m_0 = 3$; $t = 10$.

The justification for the above conclusion is that the group velocity $V_d^* = V_d^*(m_0)$ in figure 11(b) associated with the positive peak of $\text{Re}(\omega_1)$ under discussion takes on negative values for all m_0 within the first and the second ranges of the spanwise wavenumber.

According to the behaviour of the first dispersion curves in figures 6 and 7, the positive peak of $\text{Re}(\omega_1)$ is missing from the left-hand segments of both branches in the third range $5 < m_0 < 7$. This means, in effect, that the upstream-advancing wave packets of the type considered above cease to be emitted by the pulsed ribbon, even though the magnitude of $\max_d[\text{Re}(\omega_1)]$ continues to increase in figure 11(a) up to a point $m_0 = 5.3$ where the group velocity vanishes to zero. The contribution from the scarcely perceptible kink in figure 6 gets insufficient for the generation of the wave-packet-type disturbances in the upstream direction.

Figure 17 presents the wave system in front of the ribbon obtained in the computation with $m_0 = 3$. At $t = 10$, the amplitude of the largest cycle is about 3×10^4 times less than the size of pulsations in the centre of the disturbance sweeping downstream. The computed wavenumber $k = -0.46$ of the largest cycle agrees well with the corresponding theoretical value $k_d^*(3) = -0.42$. An estimate for the group velocity leads to a value $V_d^*(3) = -3.9$ in keeping with that in figure 11(b).

The upstream-propagating signal computed for $m_0 = 5$ is displayed in figure 18.

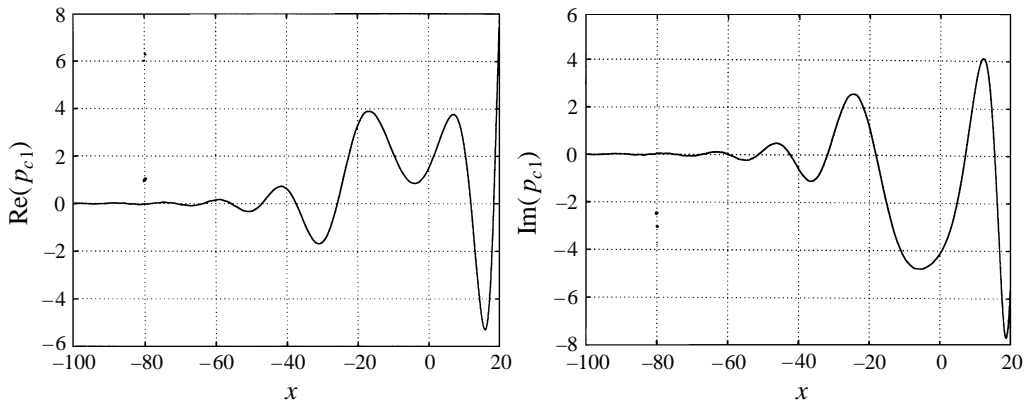


FIGURE 18. Ribbon-induced pressure distributions vs. the streamwise coordinate in the upstream-advancing wave packet for $m_0 = 5$; $t = 10$.

Exponentially growing oscillations are clearly seen ahead of the ribbon. They are induced by monotonic variations of $\text{Re}(\omega_1)$ along the left-hand segments of both branches making up the first dispersion curve in the complex ω -plane, since there is no positive peak of $\text{Re}(\omega_1)$ when $m_0 = 5.3$. In line with the above conclusion from the general analysis, the upstream signal does not take the shape of a separate wave packet, rather it is inextricably entwined with the vigorous disturbance in figure 16. This implies, in essence, that the mechanism for triggering the wave system moving against the oncoming stream drastically changes when passing through a narrow interval centred about $m_0 = 5$ and new effects come into play in the third range $5 < m_0 < 7$.

5.5. Wave packets with large values of $m_0 > 7$

When the spanwise wavenumber m_0 becomes greater than 7, an alternative mechanism controls the development of pulsations over and ahead of the ribbon. From the analysis of the first dispersion curve in the complex ω -plane summarized in figure 8 with $m_0 = 8$ we see the global and local maxima of $\text{Re}(\omega_1)$ on its lower branch to merge together and form a single smoother maximum whose strength progressively drops with m_0 increasing. The disturbance is mostly driven by a contribution from this extremum, so it propagates as a whole downstream. However, contributions from the monotonic variations of $\text{Re}(\omega_1)$ on each side of the extremum can affect the wave system to a substantial degree. The above consideration within the framework of the steepest descent method suggests that the disturbance field builds rapidly up in the vicinity of the perturbing source. The left-hand segment of the lower branch is responsible for inducing exponentially growing pulsations upstream of the ribbon. Note that the left-hand segment of the upper branch also contributes to the generation of amplifying signals in this region.

Computed results lend credence to our general views. To elucidate the new mechanism at the heart of streamwise absolute instability, two successive instants $t = 7.5$ and $t = 10$ are chosen in the computation of oscillation patterns for the same value $m_0 = 8$. Figures 19 and 20 exhibit an indivisible wave packet with rapidly increasing amplitude of pulsation cycles both downstream and over the ribbon. The tail part of amplifying disturbances is seen to penetrate the region upstream of the perturbing source. At $t = 10$ the amplitude of the wave packet is more than 10^3 times lower than the oscillation swing in the downstream-moving wave packet in figure 16. This

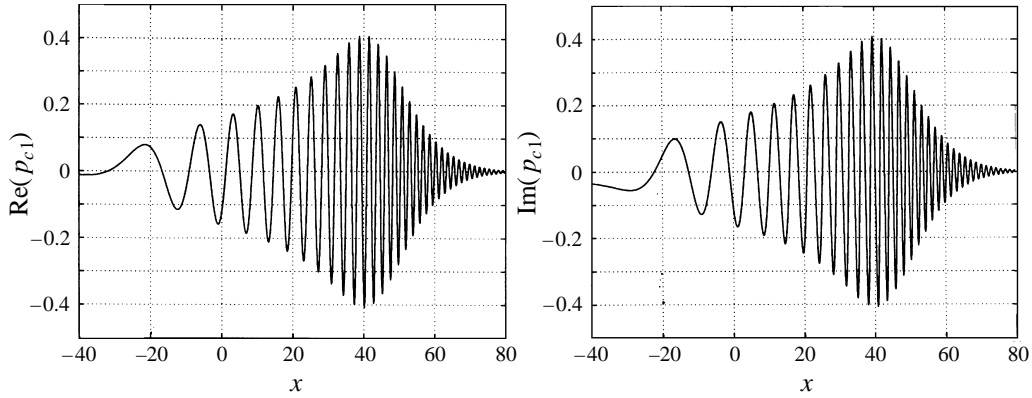


FIGURE 19. Global ribbon-induced pressure distributions vs. the streamwise coordinate for a large value $m_0 = 8$; $t = 7.5$.

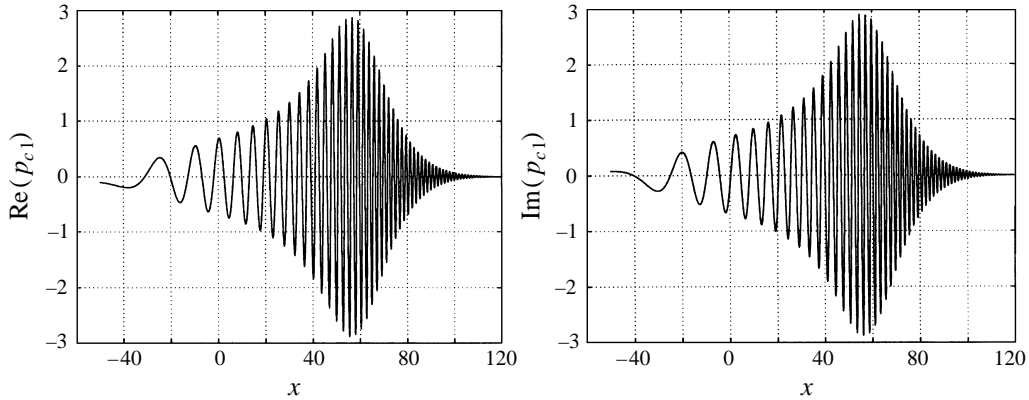


FIGURE 20. Global ribbon-induced pressure distributions vs. the streamwise coordinate for the same value $m_0 = 8$ as in figure 19 and a later time $t = 10$.

difference derives from the fact that the size of the single maximum of $\text{Re}(\omega_1)$ on the lower branch of the first dispersion curve falls off in the fourth range $m_0 > 7$ under consideration. At the same time the disturbance propagation speed increases and amounts to a value 5.8 which is yet less compared to the corresponding value $V_g^*(8) = 6.7$ of the group velocity from the plot in figure 10(b). Another distinguished feature of the disturbance in question is in the length of oscillation cycles. It monotonically increases from the front part of the wave system preceded by the oscillatory tongue towards the tail, penetrating a domain ahead of the ribbon. Long-wavelength cycles of the tail are associated with the spreading of the disturbance which is sustained by a contribution from the monotonic variations of $\text{Re}(\omega_1)$ along the left-hand segments of the first dispersion curve.

6. Discussion and conclusions

The wave packets sweeping downstream in figures 15 and 16 illustrate the development of convective instability in boundary layers. This type of disturbance amplification is well known to be fundamental to conventional routes to transition in two-dimensional shear flows. Notice, however, that highly modulated signals can

grow 10^3 – 10^4 times not far from the source of their excitation. This property makes them dissimilar to the harmonic wavetrains exploited as a rule in wind-tunnel tests. The latter disturbances require a much longer distance to be enhanced to the same amplitude unless they are chosen to be the most amplified.

On the other hand, figures 17 and 18 introduce wave packets advancing against the oncoming steam. We emphasize that the wave packet in figure 17 belongs among the most violently developing upstream disturbances. These signals can result in the flow field breakdown ahead of the pulsed ribbon. In other words, they are responsible for streamwise absolute instability of boundary layers. So far, this type of instability has not been reported in experiments with swept-wing flows. This concept sheds new light on boundary-layer physics.

The first evidence for the existence of absolutely unstable oscillations in related rotating-disk environments came recently to light in Lingwood (1995, 1996). As has been mentioned previously she advanced, using the pinching criterion from the work of Briggs (1964) and Bers (1975) on plasma physics, theoretical arguments establishing the concept of absolute instability and then substantiated her analysis by direct measurements. Apparently, the axial structure of the excited velocity field in the experimental study by Lingwood (1996) was of the type shown in figures 19 and 20 where the disturbance appears in the form of a single wave packet. The position where the trailing edge of the wave packet comes to rest on the disk is identified with the onset of transition. However, there is a significant distinction between the rotating-disk flow examined by Lingwood (1995) and the swept-wing boundary layer considered in the context of the receptivity problem (2.9), (2.10*a, b*), despite a good consensus of opinion that the former can serve as a model for the latter. It seems quite reasonable to provide, after Lingwood (1995), the initial perturbation by an impulsive circumferential line forcing. This forcing is aligned with the mainflow in a frame of reference rotating with the disk. The group velocity of an excited wave packet and crossflow are both in the radial direction. The rotating-disk boundary layer breaks down when the absolutely unstable disturbances propagating through crossflow stop at some distance from the centre of the disk. On the other hand, the receptivity problem (2.9), (2.10*a, b*) where the initial perturbation derives from the ribbon aligned with crossflow may be regarded as typical of the swept-wing boundary layer. Under these circumstances the group-velocity vector becomes parallel to the direction of the local outer stream. However the formulation in (2.9), (2.10*a, b*) involves the important limitation that the arising disturbances vary periodically in z , whereas from a point source they are free to convect in the crossflow direction. Therefore, the receptivity problem posed is indicative only of streamwise absolute instability rather than being capable of resolving the issue of absolute instability in the strict sense. As a consequence, the absolute instability evolves in the streamwise motion of a fluid due to upstream-penetrating oscillations. Recent results of Lingwood (1977) and Taylor & Peake (1998) published when the present paper was in the process of being reviewed shed light on the general problem. Using a finite-Reynolds-number approach which is based upon the pinching criterion as applied to solutions of the Orr–Sommerfeld equation, the authors of both papers argue that disturbances from a point source can be at rest in any direction falling within a certain range of flow angles since the corresponding component of the group velocity decays to zero. The other component of the group velocity in the same frame of reference takes a finite value, thereby determining the direction and speed of the disturbance drift. Thus, the three-dimensional boundary layer is prone to absolute instability only in one of two orthogonal directions, but not in both directions simultaneously. Different

mechanisms governing the development of self-excited oscillations do not come within the province of the consideration in Lingwood (1997) and Taylor & Peake (1998).

From the pure mathematical point of view, a multiplier $K^{-5/3}$ entering the expression (3.16) on the right-hand side of the dispersion relation (4.2) lies at the heart of streamwise absolute instability in a three-dimensional boundary layer. The very existence of the reduced wavenumber $K = k\tau_x + m_0\tau_z$ comes from the fact that the direction of the velocity vector across the boundary layer does not coincide with the direction of the local external stream. It is just the denominator of $Q(k, m_0; M_\infty, \varepsilon_2 D_{(zz)}; \tau_x, \tau_z)$ which causes the first dispersion curve in the complex ω -plane to split into two separate, lower and upper, branches each of which consists of two different segments merging together as shown in figure 2 for $m_0 = 0.1$. The left-hand segments are missing from the shape of the first dispersion curve in the particular case of two-dimensional disturbances with $m_0 = 0$ and $K = k\tau_x$. Both right-hand segments carry positive values of $V = -d \operatorname{Im}(\omega_1)/dk$ whilst the same derivative has negative values along both left-hand segments. We have $V = 0$ at those points where the two segments are connected to make up a single branch. Therefore, the two right-hand segments trigger convective instability well known from numerous studies on two-dimensional boundary layers. On the other hand, the two left-hand segments are associated with absolutely unstable disturbances capable of advancing upstream from the periodically shaped ribbon. The disturbances of this kind are inherent only in three-dimensional flows where coupling of travelling waves with crossflow vortices is a dominant feature controlling their amplification and determining the path to transition.

We may treat both left-hand segments as making up a specific viscous eigenmode in the complex ω -plane which falls outside the scope of the analysis in Lingwood (1997) and Taylor & Peake (1998). It is vital to note that the mode involves passing to the limit $K \rightarrow 0$. The wave fronts propagate in the direction normal to the wall shear stress in this limit. However, in view of (4.4) the formation of a critical layer at some distance from a solid surface should be taken into account when $K \rightarrow 0$. Apparently, an analogous but spatially damped inviscid mode has been indicated by Mack (1985) and Balakumar & Malik (1990) in connection with the rotating-disk boundary layer. The new mode briefly mentioned by them is central to the analysis in Lingwood (1995). The behaviour of the eigenmode comprising both left-hand segments of the first dispersion curve becomes intricate in the complex k -plane because it has branch-point singularities and cuts.

A few remarks are due now to demonstrate broad consistency between the triple-deck theory and experimental findings, accounting at the same time for the lack of direct observations on absolutely unstable disturbances in the streamwise direction. The work of Nitschke-Kowsky & Bippes (1988), Bippes *et al.* (1991), Deyhle *et al.* (1993) and Deyhle & Bippes (1996) provides firm evidence that the measured frequencies, wavelength and phase velocities fall within the range of the TS eigenmodes. Our general consideration in §§2 and 3 is based on a related high Reynolds number assumption leading to the special scalings in (2.3a–c) and (2.4a–c). Thus, the asymptotic approach under examination is in line with this part of the experimental data. The amplitude growth rates and group velocities are reported by Bippes *et al.* (1991) and Deyhle *et al.* (1993) to strongly deviate from those predicted by linear stability theory. However, this inconsistency between the two sets of observable physical quantities defining the wave system development in a three-dimensional boundary layer seems to be less surprising if we make allowance for the fact that the concept of streamwise absolute instability has been completely ignored so far. The amplification rates and

group velocities can be adequately treated only in the context of this notion in view of their extreme sensitivity to wind-tunnel test conditions. For the same reason, even the position where the crossflow vortex modes are induced strongly depends on minor scratches or dust particles on the wing surface. Careful measurements by Radeztsky *et al.* (1993) show similar effects with artificial micron-sized roughness elements placed near the attachment line. For a broader exposition of experimental data see Reed & Saric (1989), Deyhle & Bippes (1996) and Reed *et al.* (1996).

As we have seen, the shape of the left-hand segments of the first dispersion curve can vary depending on the value m_0 of the spanwise wavenumber prescribed by the ribbon (2.9). A small positive peak of $\text{Re}(\omega_1)$ starts developing in the first range $0 < m_0 < 2$ on the left-hand segment of the lower branch. In the second range $2 < m_0 < 5$ this peak amplifies to a substantial magnitude inducing the most rapidly growing wave packets upstream of the pulsed ribbon. Figure 17 gives a good idea of the disturbances in question. However, upon passing to the third range $5 < m_0 < 7$ the positive peak of $\text{Re}(\omega_1)$ starts declining and completely vanishes in the fourth range $m_0 > 7$. Weaker oscillations of the type portrayed in figures 19 and 20 are driven by continuous contributions from the monotonic variations of $\text{Re}(\omega_1)$ along the left-hand segment of the lower branch. The strong dependence of the amplitude growth rate on the spanwise wavenumber brings into being a selectivity mechanism for disturbances developing under natural conditions. The most vigorously enhancing wave patterns with $2 < m_0 < 5$ would be expected to dominate both in flight and wind-tunnel tests.

Experimental data available are consistent with this prediction. Surface-visualization techniques and hot-wire measurements reveal, as a rule, regularly spaced streaks which are aligned approximately with the mainflow direction. Let λ_x^* and δ^* designate, respectively, the spanwise wavelength and the physical boundary-layer thickness in initial dimensional variables. According to Reed & Saric (1989), the ratio λ_x^*/δ^* may be considered as a constant, nearly equal to 4, for the swept-wing boundary layer. Starting from (2.3b) we have

$$\frac{\Delta z^*}{\delta^*} \sim \frac{\pi}{m_0} \varepsilon^{-1}, \quad \varepsilon = R^{-1/8}. \quad (6.1)$$

The estimate in (6.1) is close to the above experimental value provided that $2 < m_0 < 5$.

The next question we address in connection with flight/wind-tunnel observations is how the disturbance moving against the oncoming stream can induce a streaky pattern fixed in space. In order to shed light on this issue let us evaluate the wave system at the front edge of the signal, no matter what the spanwise wavenumber m_0 . Since the limit (4.6) holds for all four ranges of m_0 , as $K \rightarrow \pm 0$, both left-hand segments of the first dispersion curve in the complex ω -plane contribute equally to amplification of the excess-pressure field. It is easily obtainable by using the Kelvin stationary-phase principle on condition that $(-x)/t \gg 1$. As a result we have

$$p_1 = -\frac{\omega_0}{(2\pi)^{1/2}} \frac{\tau_x^{1/4} B_0^{3/4}}{(k_{lim}^2 + m_0^2)^{1/4}} e^{-m_0^2 \tau_z^2 / (4\tau_x^2)} t^{3/4} (-x)^{-5/4} \cos \left[\frac{m_0}{\tau_x} (\tau_z x - \tau_x z) \right], \quad (6.2a)$$

$$B_0 = \frac{k_{lim}^2}{[(1 - M_\infty^2) k_{lim}^2 + m_0^2]^{1/2}} + \varepsilon_2 m_0^2 D_{(zz)}, \quad (6.2b)$$

where $k_{lim} = -m_0 \tau_z / \tau_x$. Clearly, this is a standing wave with the amplitude algebraically growing in time and decaying with the upstream distance from the pulsed

ribbon. The streaks in (6.2a) are $\pi\tau_x/m_0$ apart and extend in the direction of the wall shear stress rather than being aligned with the velocity of the oncoming stream. On the strength of (6.2b), $B_0 \rightarrow 0$ if $m_0 \rightarrow 0$, that is, upstream propagation vanishes when the disturbance field becomes two-dimensional. In the opposite limit $B_0 \rightarrow \infty$ as $m_0 \rightarrow \infty$, however, a multiplier $\exp[-m_0^2\tau_z^2/(4\tau_x^2)]$ damps out amplification of harmonics with large crossflow wavenumbers. A value of m_0 is likely to be forced through the selectivity mechanism discussed earlier.

The results set forth above are in sharp contrast to the disturbance propagation in the two-dimensional boundary layer on a flat plate, where the onset of transition happens suddenly but the location is nevertheless highly dependent on a particular flight/wind-tunnel environment. The linear stage of the TS wave amplification in the Blasius flow is mild and extends over a few hundred wavelengths downstream of a ribbon generating small-amplitude periodic oscillations. The TS stage shortens to several tenths of a wavelength with the ribbon operating in the pulsed mode. In general, introducing artificial disturbances into the two-dimensional boundary layer drastically changes the location of transition. The process is driven by convectively unstable disturbances which sweep downstream of a region where they were excited. The routes to transition in the three-dimensional boundary layer on a swept wing are completely dissimilar, for strong nonlinear interactions become dominant from near a chordwise position where the disturbances grew to experimentally measurable size (Bippes *et al.* 1991; Deyhle & Bippes 1996; Reed *et al.* 1996). For this reason the transition location is even more difficult to accurately determine in wind-tunnel tests with three-dimensional flow than with two-dimensional flow. The streamwise absolute instability can start from any external source to terminate in the same final state, governed by nonlinear effects, and make it insensitive to the exact form of the disturbance sources.

This scenario is inherent in a clean environment of carefully conducted experiments with fairly weak artificial disturbances. The boundary-layer breakdown is caused by primary absolutely unstable waves associated with the mean velocity profiles. Although the mean velocity profiles can have an inflection, high frequencies due to an inviscid secondary instability are not recorded under these circumstances in the rotating-disk boundary layer (Corke & Knasiak 1996; Lingwood 1996). If, however, the strength of external sources gets large enough, the secondary instabilities of the modulated base flow seem to play an important part in the onset of transition. Accordingly, the dominant mode in the wind-tunnel tests by Bippes *et al.* (1991) with a swept-wing flow could be switched from stationary to travelling when the free-stream turbulence level increased. Time series from Wilkinson & Malik (1985) clearly show secondary instabilities in the rotating-disk flow. In environments dominated by large-sized natural disturbances (free-stream turbulence patches for example) nonlinear interactions are likely coupled with the mechanism of streamwise absolute instability. A similar coupling is likely to provide an explanation for why transition in the Blasius boundary layer happens so suddenly within a short distance after the long gradual enhancement of the predominantly two-dimensional TS waves. As is well known, three-dimensionality becomes an intrinsic feature of laminar disturbances entering an essentially nonlinear stage of their development, at the threshold of breakdown.

For these reasons it is very difficult to study in wind-tunnel tests the linear range of amplification under natural conditions of transition characteristic of the boundary layer on a swept wing. Some attempts have been made to artificially stimulate the onset of three-dimensional instabilities. However, to date it has been possible to excite only the stationary vortices from roughness elements in a repeatable manner. Only

recently the travelling modes were experimentally observed to be more amplifying than the stationary modes as expected from hydrodynamic stability theory (Deyhle & Bippes 1996). Nevertheless, the growth of both modes is still overpredicted. Direct observations of absolutely unstable wave packets in the streamwise direction seem to be beyond the realm of the techniques available at present. Therefore, the measurement of group velocities offers probably the most promising way to accomplish this goal. As mentioned, significant differences in computed and measured directions ranging up to 30–40° have been reported by Deyhle *et al.* (1993). But the feasibility of streamwise absolute instability occurring was not taken into account in those computations at all. Once the discrepancy between theoretically predicted directions of the group velocity and the corresponding experimental data has been diminished, the growth rates of both stationary vortices and unsteady modes may be found to be in much closer agreement.

The authors wish to express their sincere thanks to Professor Julian D. Cole for encouraging discussions and profound comments. We are indebted also to all of the referees for their remarks and suggestions.

This work was sponsored by the Air Force Office of Scientific Research, Air Force Materials Command, USAF, under grant number F49620-97-1-0141 DEF. The US Government is authorized to reproduce and distribute reprints for governmental purposes notwithstanding any copyright notation thereon. The views and conclusions contained herein are those of the authors and should not be interpreted as necessarily representing the official policies or endorsements, either expressed or implied, of the Air Force Office of Scientific Research or the US Government. The support to E.D.T. was given by NAS under CAST grants.

REFERENCES

- ABRAMOWITZ, M. & STEGUN, I. A. 1964 *Handbook of Mathematical Functions*. National Bureau of Standards.
- ARNAL, D. & JUILLEN, J. C. 1987 Three-dimensional transition studies at ONERA/CERT. *AIAA Paper* 87-1335.
- BALAKUMAR, P. & MALIK, M. R. 1990 Travelling disturbances in rotating-disk flow. *Theor. Comput. Fluid Dyn.* **2**, 125–137.
- BENNEY, D. J. & GUSTAVSSON, L. H. 1981 A new mechanism for linear and nonlinear hydrodynamic instability. *Stud. Appl. Maths* **64**, 185–209.
- BERS, A. 1975 Linear waves and instabilities. In *Physique des Plasmas* (ed. C. Dewitt & J. Peyraud), pp. 117–215. Gordon & Breach.
- BIPPES, H., MÜLLER, B. & WAGNER, M. 1991 Measurements and stability calculations of the disturbance growth in an unstable three-dimensional boundary layer. *Phys. Fluids A*, **3**, 2371–2377.
- BREUDO, L. 1991 Three-dimensional absolute and convective instabilities, and spatially amplifying waves in parallel shear flows. *Z. Angew. Math. Phys.* **42**, 911–942.
- BRIGGS, R. J. 1964 *Electron-Stream Interaction with Plasmas*. MIT Press.
- CORKE, T. C. & KNASIAK, K. F. 1996 Cross-flow instability with periodic distributed roughness. In *Proc. IUTAM Symp. on Nonlinear Instability and Transition in Three-Dimensional Boundary Layers* (ed. P. W. Duck & P. Hall), pp. 267–282. Kluwer.
- CRIMINALE, W. O. & DRAZIN, P. G. 1990 The evolution of linearized perturbations of parallel flows. *Stud. Appl. Maths* **83**, 123–157.
- DALLMANN, U. & BIELER, H. 1987 Prediction and analysis of primary instability of a three-dimensional swept plate boundary layer. *AIAA Paper* 87-1337.
- DEYHLE, H. & BIPPES, H. 1996 Disturbance growth in an unstable three-dimensional boundary layer and its dependence on environmental conditions. *J. Fluid Mech.* **316**, 73–113.

- DEYHLE, H., HÖHLER, G. & BIPPES, H. 1993 Experimental investigation of instability wave propagation in a three-dimensional boundary-layer flow. *AIAA J.* **31**, 637–645.
- GAJJAR, J. S. B., AREBI, M. A. & SIBANDA, P. 1996 Nonlinear development of crossflow instabilities in compressible and incompressible boundary-layer flows. *AIAA Paper* 96-2159.
- GRAY, W. E. 1952 The effect of wing sweep on laminar flow. *RAE TM Aero.* 255.
- GREGORY, N., STUART, J. T. & WALKER, W. S. 1955 On the stability of three-dimensional boundary layers with applications to the flow due to a rotating disk. *Phil. Trans. R. Soc. Lond. A* **248**, 155–199.
- HUERRE, P. & MONKEWITZ, P. A. 1990 Local and global instabilities in spatially developing flows. *Ann. Rev. Fluid Mech.* **22**, 473–537.
- KACHANOV, YU. S. 1996 Experimental studies of three-dimensional instability of boundary layers. *AIAA Paper* 96-1978.
- KACHANOV, YU. S., TARARYKIN, O. I. & FEDOROV, A. V. 1990 A study of the stability of a boundary layer on a swept-wing model against stationary disturbances. *Izv. Sibirsk. Otd. Akad. Nauk SSSR, Ser. Tekh. Nauk* No. 5, 11–21 (in Russian).
- KOHAMA, Y. 1987 Some expectation on the mechanism of crossflow instability in a swept wing flow. *Acta Mech.* **66**, 21–38.
- KORN, G. A. & KORN, T. M. 1961 *Mathematical Handbook for Scientists and Engineers*. McGraw-Hill.
- LANDAU, L. D. & LIFSHITZ, E. M. 1959 *Fluid Mechanics*. Pergamon.
- LINGWOOD, R. J. 1995 Absolute instability of the boundary layer on a rotating disk. *J. Fluid Mech.* **299**, 17–33.
- LINGWOOD, R. J. 1996 An experimental study of absolute instability of the rotating-disk boundary-layer flow. *J. Fluid Mech.* **314**, 373–405.
- LINGWOOD, R. J. 1997 On the impulse response for swept boundary-layer flows. *J. Fluid Mech.* **344**, 317–344.
- MACK, L. M. 1985 The wave pattern produced by point source on a rotating disk. *AIAA Paper* 85-0490.
- MANUILOVICH, S. V. 1983 On the free interaction of a spatial boundary layer with an external potential flow. *Izv. Akad. Nauk SSSR, Mekhan. Zhidk. i Gaza* No. 5, 45–53 (in Russian; English translation: *Fluid Dyn.* **18**, 695–701, 1984).
- MESSITER, A. F. 1970 Boundary-layer flow near the trailing edge of a flat plate. *SIAM J. Appl. Maths* **18**, 241–257.
- NITSCHKE-KOWSKY, P. & BIPPES, H. 1988 Instability and transition of a three-dimensional boundary layer on a swept flat plate. *Phys. Fluids* **31**, 786–795.
- POLL, D. I. A. 1985 Some observations of the transition process on the windward face of a long yawed cylinder. *J. Fluid Mech.* **150**, 329–356.
- RADEZTSKY, R. H., JR., REIBERT, M. S. & SARIC, W. S. 1994 Development of stationary crossflow vortices on a swept wing. *AIAA Paper* 94-2373.
- RADEZTSKY, R. H., JR., REIBERT, M. S., SARIC, W. S. & TAKAGI, S. 1993 Effect of micron-sized roughness on transition in swept wing flows. *AIAA Paper* 93-0076.
- REED, H. L. & SARIC, W. S. 1989 Stability of three-dimensional boundary layers. *Ann. Rev. Fluid Mech.* **21**, 235–284.
- REED, H. L., SARIC, W. C. & ARNAL, D. 1996 Linear stability theory applied to boundary layers. *Ann. Rev. Fluid Mech.* **28**, 389–428.
- RYZHOV, O. S. & TEREENT'EV, E. D. 1984 Some properties of vortex spots in a boundary layer on a plate. *Dokl. Akad. Nauk SSSR* **276**, 571–575 (in Russian; English translation: *Sov. Phys. Dokl.* **29**, 349–351, 1984).
- RYZHOV, O. S. & TEREENT'EV, E. D. 1986 On the transition mode characterizing the triggering of a vibrator in the subsonic boundary layer on a plate. *Prikl. Matem. Mekham.* **50**, 974–986 (in Russian; English translation: *PMM USSR* **50**, 753–762, 1987).
- RYZHOV, O. S. & TEREENT'EV, E. D. 1991 Wave motions in a three-dimensional boundary layer. *Prikl. Matem. Mekham.* **55**, 912–927 (in Russian; English translation: *PMM USSR* **55**, 789–804, 1991).
- RYZHOV, O. S. & TEREENT'EV, E. D. 1996 Nonlinear waves in the three-dimensional boundary layer. In *Proc. IUTAM Symp. on Nonlinear Instability and Transition in Three-Dimensional Boundary Layers* (ed. P. W. Duck & P. Hall), pp. 167–176. Kluwer.

- RYZHOV, O. S. & TERENT'EV, E. D. 1997 A composite asymptotic model for the wave motion in a steady three-dimensional subsonic boundary layer. *J. Fluid Mech.* **337**, 103–128.
- SARIC, W. S. & YEATES, L. G. 1985 Experiments on the stability of crossflow vortices in swept-wing flows. *AIAA Paper* 85-0493.
- SMITH, F. T. 1989 On the first-mode instability in subsonic, supersonic or hypersonic boundary layers. *J. Fluid Mech.* **198**, 127–153.
- SMITH, F. T., SYKES, R. I. & BRIGHTON, P. W. 1977 A two-dimensional boundary layer encountering a three-dimensional hump. *J. Fluid Mech.* **83**, 163–176.
- SQUIRE, H. B. 1933 On the stability of three-dimensional disturbances of viscous fluid flow between parallel walls. *Proc. R. Soc. Lond. A* **142**, 621–628.
- STEWART, P. A. & SMITH, F. T. 1987 Three-dimensional instabilities in steady and unsteady non-parallel boundary layers, including effects of Tollmien-Schlichting disturbances and crossflow. *Proc. R. Soc. Lond. A* **409**, 229–248.
- STEWARTSON, K. 1969 On the flow near the trailing edge of a flat plate. II. *Mathematika* **16**, 106–121.
- TAYLOR, M. J. & PEAKE, N. 1998 The long-time behaviour of incompressible swept-wing boundary layers subject to impulsive forcing. *J. Fluid Mech.* **355**, 359–381.
- TERENT'EV, E. D. 1984 The linear problem of a vibrator performing harmonic oscillations at supercritical frequencies in a subsonic boundary layer. *Prikl. Matem. Mekhan.* **48**, 264–272 (in Russian; English translation: *PMM USSR* **48**, 184–191, 1984).
- WILKINSON, S. P. & MALIK, M. R. 1985 Stability experiments in the flow over a rotating disk. *AIAA J.* **23**, 588–595.